Seasonally Alternate Roles of the North Pacific Oscillation and the South Pacific Oscillation in Tropical Pacific Zonal Wind and ENSO

WENXIU ZHONG,[a,b,c] WENJU CAI,[d] ARNOLD SULLIVAN,[d,e] WANSUO DUAN,[b] AND SONG YANG[a,c]

[a] *School of Atmospheric Sciences, Sun Yat-sen University, and Southern Marine Science and Engineering Guangdong Laboratory (Zhuhai), Zhuhai, China*
[b] *State Key Laboratory of Numerical Modeling for Atmospheric Sciences and Geophysical Fluid Dynamics, Institute of Atmospheric Physics, Chinese Academy of Sciences, Beijing, China*
[c] *Guangdong Province Key Laboratory for Climate Change and Natural Disaster Studies, Sun Yat-sen University, Guangzhou, Guangdong, China*
[d] *Center for Southern Hemisphere Oceans Research, CSIRO Oceans and Atmosphere, Hobart, Tasmania, Australia*
[e] *School of Earth, Atmosphere, and Environment, Monash University, Melbourne, Victoria, Australia*

(Manuscript received 22 June 2022, in final form 16 February 2023, accepted 8 March 2023)

ABSTRACT: The western-central equatorial Pacific (WCEP) zonal wind affects El Niño–Southern Oscillation (ENSO) by involving a series of multiscale air–sea interactions. Its interannual variation contributes the most to ENSO amplitude. Thus, understanding the predictability of the WCEP interannual wind is of great importance for better predictions of ENSO. Here, we show that the North Pacific Oscillation (NPO) and the South Pacific Oscillation (SPO) alternate in fueling this interannual wind from late boreal winter to austral winter in the presence of background trade winds in different hemispheres. During the boreal winter–spring, the NPO registers footprints in the tropics by benefiting from the Pacific meridional mode and modulating the northwestern Pacific intertropical convergence zone (NITCZ). However, as austral winter approaches, the SPO takes over the role of the NPO in maintaining the anomalous NITCZ. Moreover, the interannual wind is further driven to the east in the positive phase of the SPO, by intensified central-eastern equatorial Pacific convection resulting from tropical–extratropical heat flux adjustments. A reconstructed WCEP interannual wind index involving only the NPO and the SPO possesses a long lead time for ENSO prediction of nearly one year. These two extratropical boosters enhance the viability of equatorial Pacific zonal wind anomalies associated with the large growth rate of ENSO, and the one in the winter hemisphere seems to be more efficient in forcing the tropics. Our result further indicates that the NPO benefits a long-lead prediction of the WCEP interannual wind and ENSO, while the SPO is the dominant extratropical predictor of ENSO amplitude.

SIGNIFICANCE STATEMENT: ENSO is closely linked to the interannual variability of equatorial Pacific zonal wind, and ENSO prediction is impeded by the weak predictability of the wind. We have found that the North Pacific Oscillation and the South Pacific Oscillation take turns in affecting the interannual variability of the zonal wind from the late boreal winter to austral winter, and the winter hemisphere extratropical booster is more efficient in modulating tropical convection and the associated surface winds. An estimated zonal wind index constructed by the two extratropical precursors possesses a long lead time for ENSO prediction. Our result provides useful information for better predicting ENSO by further considering winter hemisphere extratropical climate variability.

KEYWORDS: ENSO; Monsoons; Pacific Ocean; Climate variability; Seasonal cycle

1. Introduction

Equatorial Pacific zonal wind is a dominant factor that influences the evolution of El Niño–Southern Oscillation (ENSO; Bjerknes 1969). El Niño, the warm phase of ENSO, is usually accompanied by a strengthened and eastward extended anomalous westerly wind that slackens the Walker circulation (Yu et al. 2003; Tziperman and Yu 2007). Particularly, strong westerly wind events over the western-central equatorial Pacific (WCEP), defined as westerly wind bursts (WWBs), have attracted substantial research interest due to their significance to ENSO predictability (Luther et al. 1983; McPhaden et al. 1992; Harrison and Vecchi 1997; Mo 2000; Chen et al. 2015; Lian et al. 2018; Fu and Tziperman 2019). The causes of these extreme westerly wind anomalies have been investigated within the tropics (e.g., Fu and Tziperman 2019). They could be related to high-frequency atmospheric variations such as the Madden–Julian oscillation (Zhang 1996; Fasullo and Webster 2000; Kessler and Kleeman 2000; Hendon et al. 2007) and tropical cyclones (Keen 1982; Lian et al. 2019). Although with short durations (no longer than 30 days), WWBs are considered a stochastic forcing for downwelling Kelvin waves, especially for strong El Niño events (McPhaden et al. 1992;

Denotes content that is immediately available upon publication as open access.

Corresponding authors: Song Yang, yangsong3@mail.sysu.edu.cn; Wenxiu Zhong, zhongwx9@mail.sysu.edu.cn

DOI: 10.1175/JCLI-D-22-0461.1

Kessler et al. 1995; Seiki and Takayabu 2007; Chiodi et al. 2014). These eastward-propagating equatorial oceanic waves warm the eastern Pacific subsurface. Then, the consequent sea surface temperature (SST) variations enhance central-to-eastern tropical Pacific convection to the east of wind anomalies, which in turn strengthens the anomalous westerly wind and leads to a large growth rate of El Niño (Eisenman et al. 2005; Cai et al. 2020). Thus, the changes in the equatorial surface zonal wind not only reflect the perturbation caused by convection, but also modulate the underlying upper ocean, coupling ocean, and atmosphere through multiplicate feedback loops (Bjerknes 1969; Cai et al. 2012, 2015, 2020; Timmermann et al. 2018). However, predictions of ENSO relying on the WCEP zonal wind are still impeded by the weak predictability of the wind itself and by a lack of insight into its efficiency on SST variations (Bergman et al. 2001; Gebbie and Tziperman 2008; Seiki et al. 2011; Christensen et al. 2017; Tan et al. 2020).

More recently, it has been revealed that the WCEP zonal wind has a broad spectrum and contains variances in different frequencies, supposing the wind is partially stochastic (Roulston and Neelin 2000; Capotondi et al. 2018; Sullivan et al. 2021). For variations in ENSO, the low-frequency components (interannual and lower-frequency ones) are more significant than the high-frequency components (Sullivan et al. 2021). On a low frequency of the interannual time scale, the WCEP zonal wind has been linked to extratropical signals which interact with ENSO (Lau and Yang 1996; Chang et al. 2007; Vimont et al. 2009; Ding et al. 2015, 2017; Min et al. 2017; Chen and Wu 2018; Pegion et al. 2020; Min and Zhang 2020). Thus, it is of great importance to understand the formation of the low-frequency wind and its connections with the extratropics, rather than regarding the wind as a noise that responds to ENSO-developing feedback within the tropics, for better predictions of ENSO.

Extratropical monsoon systems can interact with ENSO by perturbing tropical convection (Webster and Yang 1992; Xu and Chan 2001; Zhun and Chen 2002; Li and Yang 2017; Li et al. 2021). It has been pointed out that the seasonally varying meridional monsoon flows and the zonal Walker circulation are likely coupled within the tropics (Webster and Yang 1992). In particular, the Indo-Pacific Ocean is a dominant monsoon region that also hosts ENSO. An atmospheric low-level meridional flow to the east of the Australian continent, referred to as the Australian cross-equatorial flow (ACEF; Xu and Chan 2001), moves across the equator and merges into the northwestern Pacific intertropical convergence zone (NITCZ; Stephens et al. 2007). The ACEF is an important component of the Asian–Australian monsoons. It transports cold air mass and high vorticity from the Southern Hemisphere midlatitudes to the tropics and perturbs convection by regulating atmospheric stability (Xu and Chan 2001; Stephens et al. 2007; Hong et al. 2014). On the other side of the equator, the East Asian winter monsoon (EAWM) in the Northern Hemisphere also affects tropical convection and surface winds (Chu 1988; Li 1990; Li and Li 2014). A strengthened EAWM will promote tropical convection and the occurrence of strong WCEP westerly wind anomalies during the El Niño onset time (Xu and Chan 2001). These relationships between the Asian–Australian monsoon system and tropical atmospheric variability indicate that the monsoon flows may be the important pathways whereby the extratropical climate signals affect the ENSO remotely. A recent study has proposed that both the EAWM and the ACEF could regulate the seasonal variation of the WCEP zonal wind, especially in the late boreal spring (Sullivan et al. 2021). However, whether the monsoon systems can influence the low-frequency WCEP zonal wind related to ENSO amplitude is still unclear.

In addition to the monsoon, wintertime extratropical climate variability [such as the North Pacific Oscillation (NPO; Rogers 1981)] and the tropical Pacific surface winds in the following season can be linked by the seasonal footprinting mechanism (SFM; Vimont et al. 2003a,b). This process is described by the Pacific meridional mode (PMM; e.g., Chiang and Vimont 2004). The North Pacific meridional mode (NPMM) can influence the central Pacific air–sea couplings (Chang et al. 2007; Yu et al. 2010; Chen and Wu 2018). In the positive phase of the NPMM, warm SST anomalies (SSTAs) south of Baja California initiate anomalous southwesterly wind that weakens trade winds and reduces evaporation, which decreases heat release from the ocean into the atmosphere, locally warming the underlying sea surface. This positive feedback loop involving surface wind, evaporation, and SST is referred to as the wind–evaporation–SST (WES) mechanism (Xie and Philander 1994). Through the WES feedback, the PMM is thought to propagate from the subtropics to the equatorial Pacific (Vimont et al. 2001, 2003a,b, 2009; Anderson 2007; Amaya et al. 2019). Being analogous to the NPO, a meridional dipole mode of sea level pressure anomalies (SLPAs) has been recognized as dominating the South Pacific subtropical atmospheric variability (You and Furtado 2017). It was named the South Pacific Oscillation (SPO), which can generate the South Pacific meridional mode (SPMM) adjacent to the South American coast, farther eastward than the NPMM (You and Furtado 2018, 2019; Liguori and Di Lorenzo 2019). Ding et al. (2015) and Zhang et al. (2014) proposed that the NPMM and the SPMM could similarly affect the equatorial Pacific SST. However, several other studies argued that the SPMM influenced ENSO by modulating the South American coastal upwellings and the eastern Pacific subsurface inflows, rather than via the WES mechanism (You and Furtado 2017; Liguori and Di Lorenzo 2019). They challenged the way that the SPMM affected ENSO variations as depicted by other studies, indicating that the extratropical atmospheric signals in the Northern Hemisphere and the Southern Hemisphere may influence tropical climate in different ways. How the Southern Hemisphere extratropical atmospheric signals interact with tropical climate variations on the interannual time scale needs further investigation.

Extratropical climate signals in both the Northern Hemisphere and the Southern Hemisphere can modulate tropical convection and the associated responses in surface winds. However, some key points still need to be clarified: (i) The ACEF in the western Pacific can perturb tropical convection and influence ENSO behaviors, while the SPMM in the east can initiate tropical responses as well (Xu and Chan 2001; Stephens et al. 2007; Hong et al. 2014; Ding et al. 2015; You and Furtado 2017, 2019; Larson et al. 2018). Are these processes related to each other? What are the dynamic–thermodynamic processes that dominate the tropical–extratropical interactions

in the two hemispheres and how do they compare with those proposed by previous studies? (ii) It is widely recognized that the winter hemisphere atmospheric variability is more efficient in affecting tropical convection than the summer hemisphere variability, indicating that the climate signals in the two hemispheres might affect the tropics following the seasonal cycle. However, how does the extratropical variability in the two hemispheres take turns in affecting tropical convection, and what is the relative contribution of the two hemispheres? These issues still complicate the predictions of equatorial Pacific winds and the consequent changes in SST.

Our study shows a seasonally alternating role of the NPO and the SPO in the interannual variability of the WCEP zonal wind, which largely contributes to the tropical central-eastern Pacific SST variations. We organize the paper as follows. Section 2 introduces the data and methods used in this study. Section 3 describes how the NPO and the SPO take turns in affecting tropical air–sea interactions from late boreal winter to austral winter. In section 4, we further investigate the mechanisms for the interannual WCEP zonal wind variability corresponding to the NPO and the SPO. It is shown that the two extratropical boosters fluctuate the interannual wind by perturbing tropical convection. Section 5 proposes a statistically predicted monthly WCEP zonal wind index based on the impacts of the NPO and the SPO. This reconstructed wind index with the two external atmospheric precursors possesses significant correlations with central-eastern Pacific SST variability, with a lead time of one year. It will be seen that the NPO is beneficial for a long-lead prediction of the interannual wind and ENSO, and the SPO is the most important extratropical predictor of ENSO amplitude. Section 6 summarizes the external effect of the NPO and the SPO on the variance of WCEP interannual wind and ENSO.

2. Data and methodology

a. Data

The reanalysis data from the National Centers for Environmental Prediction–National Center for Atmospheric Research (NCEP–NCAR; Kalnay et al. 1996) covering 73 years from January 1948 to December 2020 have been primarily used in this study. We use monthly-mean sea level pressure (SLP), 10-m winds, and latent heat flux gridded onto a 1° latitude–longitude grid. In addition, the daily surface zonal wind derived from the NCEP–NCAR reanalysis is used to obtain wind indices in this study. The SST dataset from the Hadley Centre Sea Ice and SST dataset (HadISST; Rayner et al. 2003) is applied to define the ENSO index, and the NOAA 1/4° daily Optimum Interpolation Sea Surface Temperature (OISST; Reynolds 1993) is obtained to explore the contribution of different frequencies of the WCEP zonal wind to the tropical Pacific SST variance. Anomalous values are calculated based on subtracting the climatological mean from the raw data. We obtain the climatological precipitation by using the CPC Merged Analysis of Precipitation (Xie and Arkin 1997), the Global Precipitation Climatology Project version 2.3 (Adler et al. 2003) combined precipitation climatology, and the precipitation rate from the NCEP–NCAR reanalysis. The tropical Pacific climatological rainfall band shown in this paper is represented by an average of the three products, from 1979 to 2011.

b. Methodology

1) EEMD

The empirical mode decomposition (EMD) is a technique that decomposes a signal into oscillatory contributions (Huang et al. 1998). By using the EMD, the original signal can be naturally decomposed into a series of modes with different dominant frequencies, referred to as intrinsic mode functions (IMFs). The EMD is fully data driven and does not require any predetermined basis functions (Huang et al. 1999). Although the EMD possesses obvious advantages in signal analysis, there are unavoidable defects such as the boundary effect and the mode-mixing effect (Wu and Huang 2009). Then, an ensemble empirical mode decomposition (EEMD) with white noise (the expectation of white noise is equal to zero) was added to the data before applying the EMD analysis was proposed (Wu and Huang 2004, 2009). The effect of adding white noise will be offset by the mean of the ensemble IMF. Therefore, the decomposition using EEMD not only keeps the inherent feature of the original signal, but also overcomes the defect of mode mixing. Previous studies have detailed how to employ the EMD and the EEMD (e.g., Flandrin et al. 2004; Rilling and Flandrin 2008; Chu and Huang 2020).

In this study, the EEMD is applied based on the NCAR Command Language (https://www.ncl.ucar.edu/Applications/eemd.shtml) as a filter to obtain the intrinsic modes of the WCEP (5°S–5°N, 135°E–180°) zonal wind with different frequencies. Then, 12 intrinsic modes can be obtained, as shown by Sullivan et al. (2021). That wind variation contains prominent interannual variations (IMFs 9–10), which largely contribute to the tropical Pacific SST variability and are used in the present study. We also compare the IMFs 9–10 with a filtered interannual wind index (1–9-yr bandpass) based on the Fourier transformation. These two interannual variations are significantly correlated, with a correlation coefficient of 0.89 (not shown). This feature means that the choice of the wind index will not change our result.

2) THE WCEP INTERANNUAL WIND

The sum of IMFs 9 and 10 (Fig. 1a) is used to represent the interannual WCEP zonal wind variance, which is referred to as interannual wind in this paper. Compared with the higher-frequency winds, the interannual wind contributes more to the central-eastern tropical Pacific SST variance (Figs. 1b,c). We focus on the interannual zonal wind in this study, as it significantly leads ENSO by 3 months. In particular, the interannual wind index (IWI, which represents the IMFs 9–10 in the following discussion) possesses the largest variance in August (Fig. 1d).

3) DEGREES-OF-FREEDOM CALCULATION

As a bandpass filter has been adopted in this study, the time series would have significant autocorrelations. We calculate the effective degrees of freedom (EDF) to test the significance of

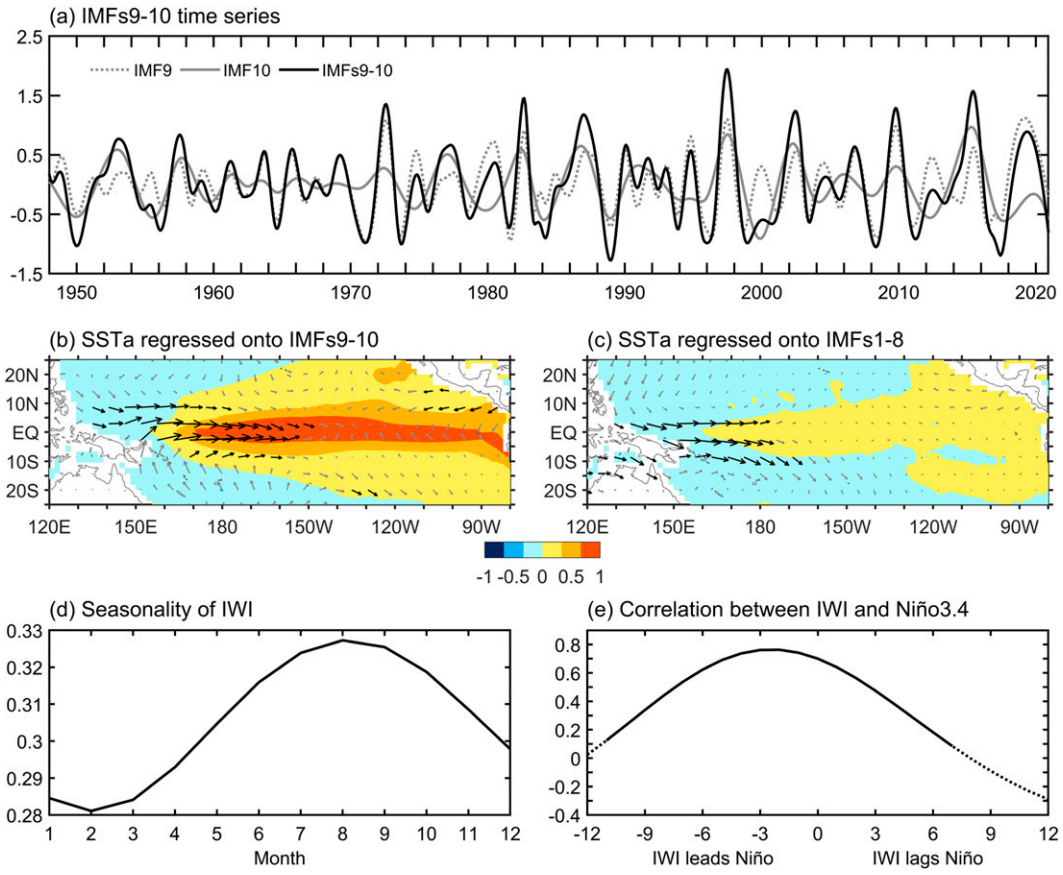

FIG. 1. Interannual components of the WCEP zonal wind. (a) Time series of IMF 9 (gray dotted line), IMF 10 (gray solid line), and IMFs 9–10 (black line, the interannual-wind index, IWI). (b) Regression patterns of daily SSTAs (shading; °C) and surface wind anomalies (vectors; m s^{-1}; zonal wind speed over 0.5 m s^{-1} is presented in black) onto the IWI and (c) higher-frequency component (IMFs 1–8). (d) Seasonality (seasonal phase locking) of the IWI. (e) Lead–lag correlations between monthly IWI and Niño-3.4. Correlation coefficients above the 90% confidence level based on the two-tailed Student's t test are connected by a solid line.

correlations between independent time series (Bartlett 1935). For two signals with lag-one autocorrelation r_1 and r_2, the EDF formula can be expressed as

$$N^* = N\frac{1 - r_1 r_2}{1 + r_1 r_2},$$

where N is the original window length, and N^* is the effective degrees of freedom in terms of the two signals.

4) THE NPO

There exist various definitions of the NPO index (Wallace and Gutzler 1981; Linkin and Nigam 2008; Yu and Kim 2011; Furtado et al. 2012; Park et al. 2013), which perform differently in reflecting tropical–extratropical interactions. In this paper, we define the NPO index based on the weighted empirical orthogonal function (EOF) following Linkin and Nigam (2008), as it can more clearly show the NPO–ENSO connection (Chen and Wu 2018). It is referred to as the NPO_{EOF} in this study, which is the second EOF mode of SLPAs over the North Pacific domain (20°–85°N, 120°E–120°W). The NPO pattern features a meridional dipole structure of the North Pacific SLPAs (Fig. 2a). This NPO index shows a large spectral power at interannual time scales (not shown). We also derive another NPO index (NPO_{NS}) using the difference in SLPAs between the positive (the northern domain in Fig. 2b) and negative (the southern domain in Fig. 2b) poles. The NPO, peaking during boreal winter, is related to other North Pacific climate patterns. In particular, the NPO variability leads the Victoria mode, the PMM, and western North Pacific patterns by at least 1 month (Ding et al. 2015).

5) THE SPO

A prominent mode of the South Pacific atmospheric variability can be obtained by applying a weighted EOF analysis on the monthly SLPAs over the southeastern Pacific domain (45°–10°S, 160°–70°W; You and Furtado 2017). This leading mode is referred to as the SPO (Fig. 2c), and it explains most of the total variance of the low-level barometric fluctuation in the South Pacific (46.6%), with the power spectrum peaking

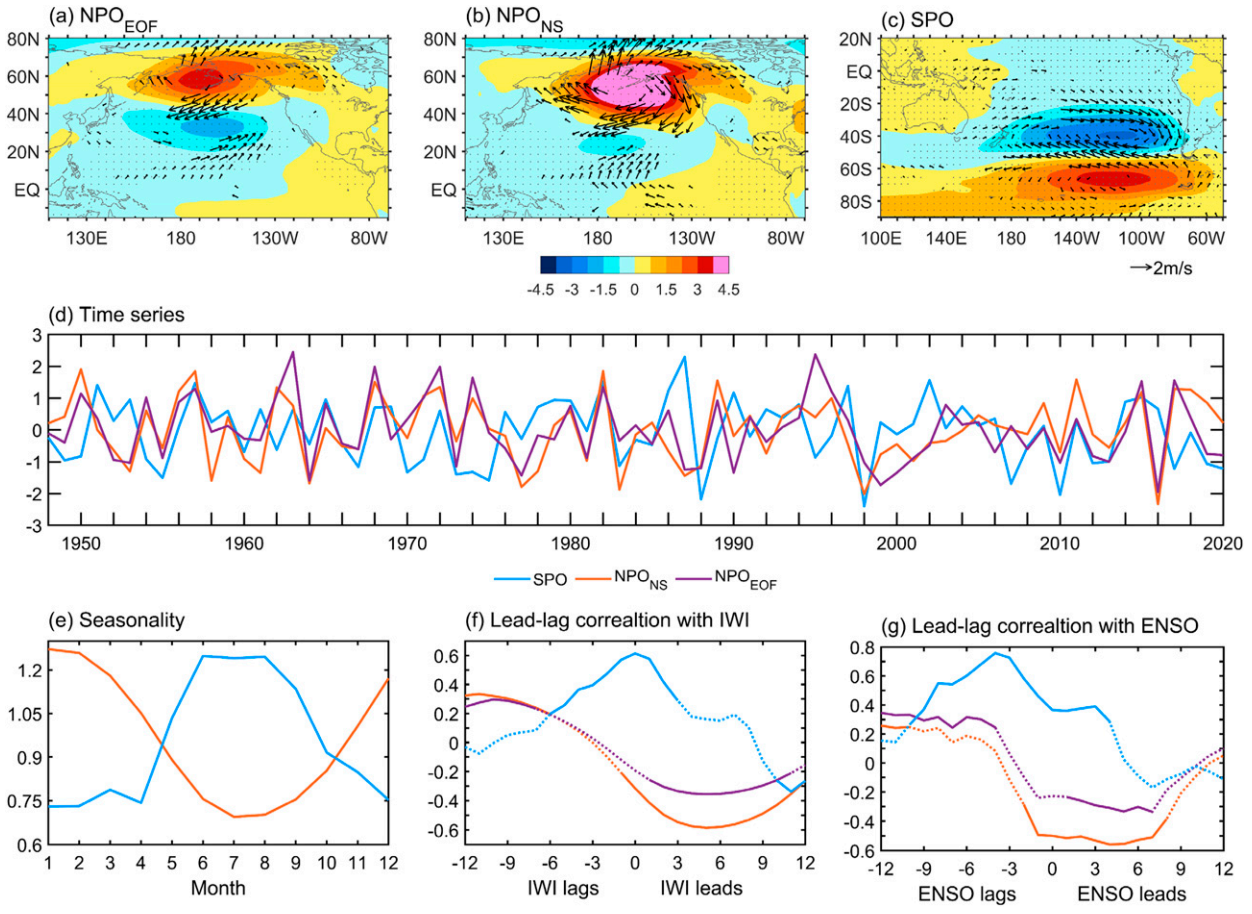

FIG. 2. Regression patterns of interannual SLPAs (hPa; shading) and 10-m wind anomalies (m s^{-1}; vectors) onto the standardized (a) NPO_{EOF} index (time series of the second EOF mode of SLPAs over the North Pacific domain 20°–85°N, 120°E–120°W), (b) NPO_{NS} index (differences in the northern domain 45°–65°N, 180°–140°Wand the southern domain 15°–35°N, 165°E–140°W in SLPAs), and (c) SPO index (time series of the first EOF mode of SLPAs over the southeastern Pacific domain 45°–10°S, 160°–70°W). (d) Time series of the three indices above (NPO_{EOF} in violet, NPO_{NS} in orange, and SPO in blue). (e) Seasonality of the monthly NPO_{NS} and SPO indices. (f) Lead–lag correlations between the NPO (SPO) and IWI (JAS-IWI). (g) As in (f), but for correlations between the NPO (SPO) and Niño-3.4 (DJF-Niño-3.4). Correlation coefficients significantly above the 90% confidence level are connected by a solid line. In (a)–(c), the statistically significant correlation coefficient of SLPAs and the NPO/SPO index is represented by stippling, and only the statistically significant correlation coefficients of 10-m winds and the NPO/SPO index are plotted (at the 90% confidence level). All correlations in this study are based on the two-tailed Student's *t* test.

on both interannual and interdecadal time scales. We only focus on interannual behaviors in this study. The anomaly patterns from regression onto the NPO and the SPO indices are derived after applying a bandpass filter of 1–9 years.

The SPO is highly correlated with ENSO, yielding a lead time of 4 months (with a correlation coefficient of nearly 0.8 (Fig. 2g), which is also shown in You and Furtado 2017). The SLP regression pattern over the full South Pacific onto the SPO is similar to the Pacific–South American pattern (PSA; Karoly 1989; You and Furtado 2017). Although the PSA is significantly correlated with ENSO (~0.3), the correlation coefficient is smaller than that between the SPO and ENSO (Fig. 2g, blue line). This feature implies that the SPO is more efficient in modulating tropical climate variability than the PSA, despite the fact that they are simultaneously related to each other with a correlation coefficient of approximately 0.4. That is, the austral winter SPO can be regarded as a key predictor for ENSO events. We will discuss how the NPO and the SPO alternate in driving the interannual WCEP zonal wind variability in this paper.

3. Extratropical systems related to the WCEP interannual wind

The WCEP interannual wind peaks around August and leads ENSO by approximately 3 months with a relatively high correlation coefficient above 0.75 (Figs. 1d,e). That is, the interannual wind can affect the growth of ENSO events, especially during its peak season in the late boreal summer. Thus, investigating the origin of this low-frequency zonal wind is

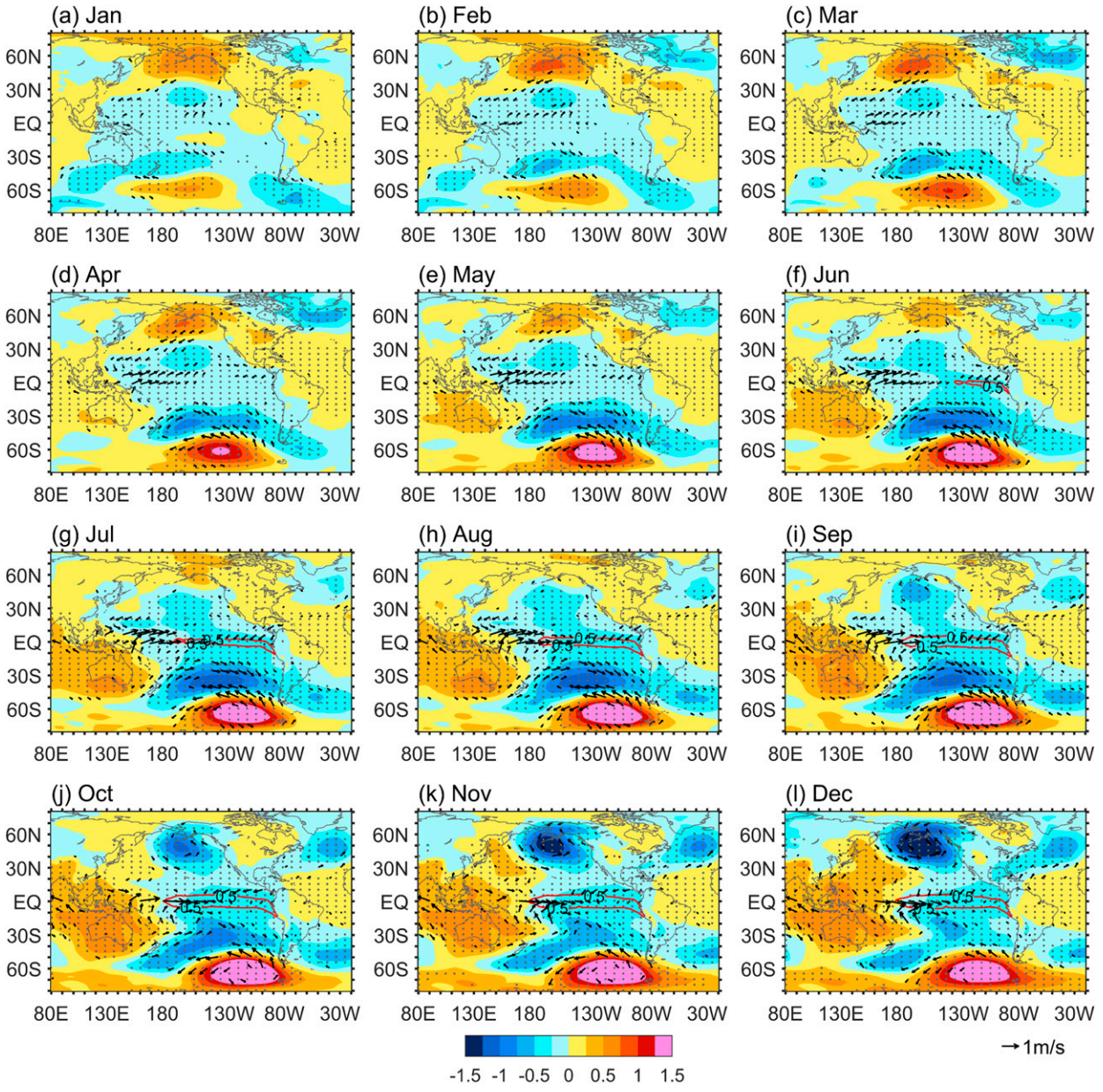

FIG. 3. Lead–lag regression patterns of interannual SLPAs (hPa; shading), SSTAs (°C; contours), and 10-m wind anomalies (m s^{-1}; vectors) onto JAS-IWI (throughout 1948–2020). (a)–(g) Lead regressions, (h) simultaneous regressions, and (i)–(l) lag regressions. The statistically significant correlation coefficient of SLPAs and the NPO/SPO index is represented by stippling, and only significant correlation coefficients of 10-m winds and the NPO/SPO index are plotted (at the 90% confidence level).

important for improving ENSO prediction. The IWI in July–September (JAS) is applied to represent the intensity of interannual wind variance. To investigate the possible impacting factors of the WCEP interannual wind, we perform lead–lag regressions of interannual SLP, SST, and surface wind onto the normalized wind index, which are shown in Fig. 3.

The North Pacific SLP variance is significantly correlated with the JAS-IWI in the boreal winter–spring, featuring an NPO-like pattern (Figs. 2a,b and 3a–c). The anomalous cyclonic surface flows over the subtropical North Pacific initiate southwesterly wind anomalies to its southern flank, indicating an NPMM pattern that can trigger central equatorial Pacific westerly wind anomalies. These anomalous equatorial WCEP zonal winds can persist to the following season despite the NPO-like pattern beginning to decay after March (Figs. 3d–f). The associated dynamics will be discussed in the next section.

In the austral winter, the JAS-IWI high-impact center moves to the Southern Hemisphere (Fig. 3). A subtropical meridional dipole pattern that is significantly correlated with the JAS-IWI exists in the South Pacific extratropics, especially in

the IWI peak season (Figs. 3g–i). This anomalous SLP pattern resembles the SPO mode. We also notice another anomalous center over the Australian continent (Figs. 3f–l). The positive SLPAs over the Indo-Australian region indicate an intensified Australian high (the Australian continent is controlled by a high pressure system in austral winter; see Fig. A1 in the appendix). Between the anomalous Australian high pressure and the SPO-related low pressure in the subtropics, there exist strengthened equatorward flows, representing a stronger ACEF (Figs. 3e–h).

The correlation coefficient between the JAS-IWI and the SPO index reaches up to 0.6, higher than that for the NPO (Fig. 2f),which indicates a stronger connection between the tropics and the South Pacific extratropics. After September, the northern lobe of the SPO-like pattern begins to tilt and fade, while North Pacific atmospheric variability becomes significantly related to the prior JAS-IWI again (Figs. 2f and 3i–l). An intensification of the Aleutian low can be seen 3 months after the IWI peak season, consistent with a mature ENSO phase in boreal winter, reflecting a significant impact of tropical climate variability on the North Pacific climate (also shown in Yeh and Kirtman 2004; Stuecker 2018; Paek et al. 2019). The above feature has shown seasonally alternate roles of the North Pacific and South Pacific extratropical atmospheric variability in the equatorial Pacific zonal wind. Next, we will discuss how the NPO and the SPO drive the tropical Pacific interannual wind.

4. Mechanisms

a. *Impacts from the NPO*

The prior boreal winter NPO is positively correlated with the succeeding ENSO, leading by 10–11 months (Fig. 2f). The equatorward lobe features a cyclonic circulation, generating southwesterly wind anomalies to the southwestern flank in the tropical central Pacific (Figs. 2a,b and Figs. 4a–e). These wind anomalies weaken the northeasterly trade winds and induce positive downward latent heat flux into the underlying sea surface (Figs. 4a–f). Then, the warming center gradually moves toward the equator in the following season, acting like a typical seasonal footprinting process (Vimont et al. 2003a,b; Chiang and Vimont 2004). Thus, the WES feedback dominates the NPO-IWI connections and triggers the WCEP interannual wind during boreal winter–spring.

We further notice that the NPO is favorable for tropical northwestern Pacific convection from January to May (Figs. 4a–c), with an anomalous rainfall center located further north than the climatological rainfall band, indicating an intensification and northward movement of the NITCZ (Figs. 4b–e). The equatorward low-pressure lobe induces asymmetric heating to the equator and boosts cross-equatorial winds, reinforcing the NITCZ through the Gill response (Gill 1980). This process also exerts southwesterly wind in the western equatorial Pacific and promotes northward ACEF (the northward ACEF starts to prevail in the western Pacific after March; Fig. A1). More latent heat flux released from the sea surface can be observed right to the east of Papua New Guinea, which reinforces the NITCZ to the north. A cluster of westerly wind anomalies occurs across the western-central equatorial Pacific, mostly located to the north of the equator (also see Kug et al. 2009). Amaya et al. (2019) illustrated the significant impact of the ITCZ on equatorial central Pacific zonal wind through the summer deep convection response to the PMM. They proposed that changes in the tropical convection took over the role of WES feedback in prior seasons and maintained the WCEP westerly wind anomalies to the boreal summer. However, we find that these NPO-related changes in the NITCZ start to decay after May (Figs. 4d–f), while the IWI-related convection anomalies are contrastingly strengthened (Fig. 5). This feature signifies that the changes in boreal summertime NITCZ and equatorial zonal wind anomalies could be induced by other factors besides the NPO. Next, we will discuss the influences of South Pacific climate variability on the tropics.

b. *Impacts from the SPO*

The SPO is the dominant mode of South Pacific atmospheric variability that peaks in the austral winter (Fig. 2e). It represents a meridional dipole pattern of SLPAs in the southeastern Pacific and explains 46.6% of the total variance (Fig. 2c). The SPO shows substantial variations on both interannual and multidecadal time scales (not shown) and is significantly correlated with the JAS-IWI (Fig. 2f), with a correlation coefficients peak (~0.6) in austral winter. The positive phase of the SPO indicates an intensification of the Australian high and an overall attenuation of the subtropical SLP to the west of the South American coast (Fig. 2c). The broad range of this anomalous pattern potentially implies a wide-range impact of the SPO on both the western Pacific close to Australia and the eastern Pacific next to South America.

The SPO starts to exert its impact on the ACEF prevailing over the western tropical Pacific as the austral winter approaches (Fig. 6). In the positive phase of the SPO, the South Pacific subtropical west–east SLP gradient modulated by both the Australian high and the southeastern Pacific low pressure is intensified (Fig. 2c), which is conducive to a stronger ACEF (due to the geostrophic effect). It can be seen that the ACEF changes simultaneously with the subtropical SLP gradient (Fig. 7, red line). After late boreal spring, the northward ACEF supported by the increasing variance of the SPO enhances the background wind speed and sea surface evaporation in the southwestern tropical Pacific (Figs. 6f–i). These processes cool the underlying sea surface and stabilize the lower troposphere to the south of the western Pacific tropical rainfall band. The SPO-related strengthened ACEF reinforces the prior NPO-induced NITCZ anomalies to the north of the equator in austral winter (Figs. 6f–h) despite the fact that the effect of the NPO is much weaker at this time (Figs. 4e–h). Therefore, the SPO variability is favorable for the persistence of equatorial westerly wind associated with the NPO-induced NITCZ (Fig. 7, gray and yellow lines).

In the southeastern Pacific, the anomalous cyclonic circulation of the SPO reduces the trade wind and excites the SPMM. Positive latent heat flux into the southeastern Pacific sea surface first appears in May of the year, as soon as the northern cyclonic lobe extends to the vicinity of Chile (Fig. 6e). As the SPO strengthens after May, anomalous northwesterly wind

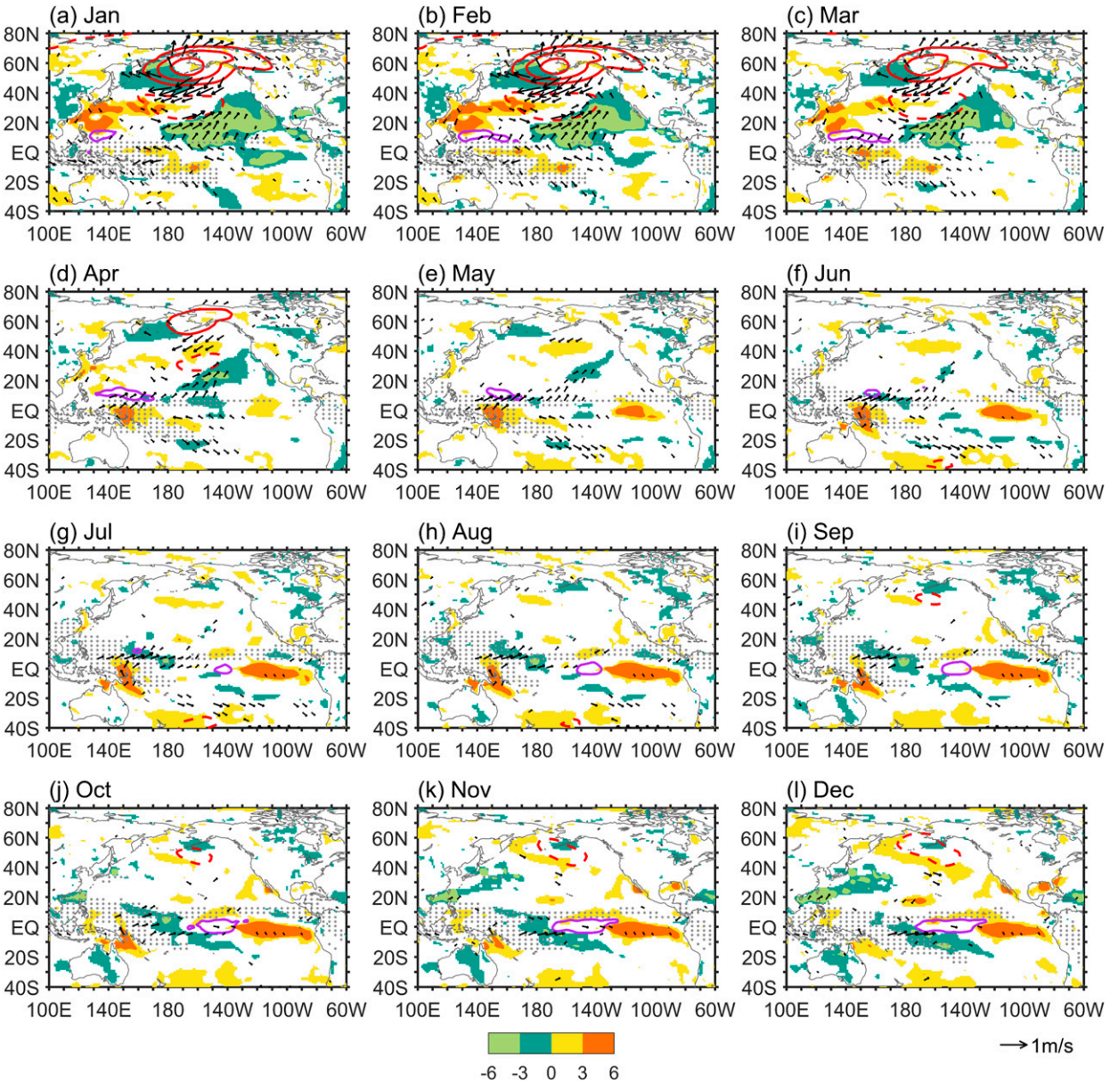

FIG. 4. Lead–lag regression patterns of interannual latent heat flux anomalies (W m^{-2}; shading; upward positive), SLPAs (hPa; red contours, solid for positive values and dashed for negative values, with an interval of 0.5), convective precipitation anomalies (mm day^{-1}; violet contours; only 0.4 mm day^{-1} is plotted), and 10-m wind anomalies (m s^{-1}; vectors) onto NPO_{EOF}. Climatological convective precipitation over 6 mm day^{-1} is indicated by gray dots. Only correlation coefficients significantly exceeding the 90% confidence level are plotted.

further weakens the southeasterly background wind and heats the underlying sea surface (Figs. 6e–h). Anomalous downward heat fluxes gradually move from the southeastern subtropical Pacific toward the central equatorial Pacific. The positive downward heat flux is confined to the south of 10°S before August. But as the background southerly wind speed is enhanced in July–September (shown in Fig. A1), it extends northward to the equator (Figs. 6h,i). The SPMM allows a seasonal footprint of the South Pacific subtropical climate signal in the tropics (also shown in Ding et al. 2015, 2017; You and Furtado 2017, 2018). Noting the obvious loss of sea surface heat induced by the strengthened ACEF, we speculate that the SPMM can drive an equatorward shift of the climatological rainband in collaboration with the ACEF (Figs. 5h,i and 6h,i).

The mutual effects of the SPO-related eastern Pacific SPMM and western Pacific ACEF induce an eastward extension of the interannual wind in austral summer, via basin-scale surface latent heat flux adjustments. In the positive phase of the SPO, the anomalous southeastern Pacific cyclonic circulation features a northward flow on its western flank, which

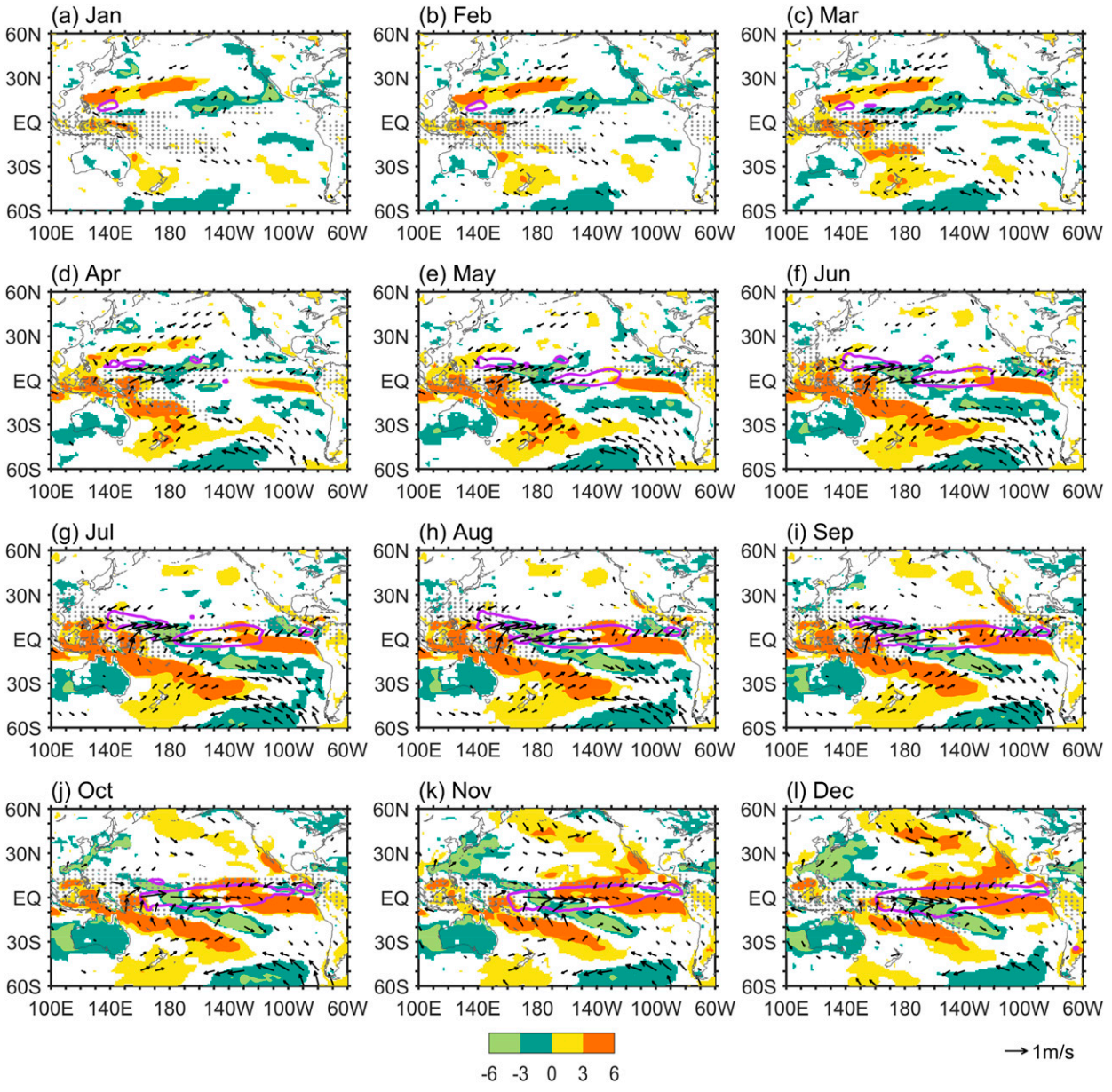

FIG. 5. Lead–lag regression patterns of interannual latent heat flux anomalies (W m^{-2}; shading; upward positive), convective precipitation anomalies (mm day^{-1}; contours; only 0.4 mm day^{-1} are plotted), and 10-m wind anomalies (m s^{-1}; vectors) onto JAS-IWI. Climatological convective precipitation over 6 mm day^{-1} is indicated by gray dots. Shading and vectors are plotted only for the values significantly exceeding the 90% confidence level.

veers around to the east as a southward flow (Figs. 6f–i). As both the ACEF and the SPO intensify in austral winter, the western Pacific sea surface loses heat, whereas the east gains heat. In Fig. 6, the positive heating center is located to the northeast of the South Pacific convergence zone (SPCZ) rainfall band, whereas the negative center is to the south. Thus, the SPO-related cyclonic circulation interacts with the background southeasterly wind through the WES effect, enhancing the heat loss in the western flank but weakening it in the eastern flank. These two processes conspire to lead to an eastward and equatorward shift of the climatological rainband (Fig. 6h), consequently promoting an eastward extension of the WCEP zonal wind anomalies. In the far-eastern Pacific (east of 130°W), downward latent heat flux into the sea surface is constrained to the south of 10°S (Fig. 6). Thus, the SPMM imprint may not influence the eastern equatorial Pacific SST directly by the WES feedback (which has been speculated in previous research, e.g., You and Furtado 2019) but via modulating the tropical convection and the associated zonal wind fluctuations, particularly during austral winter. This

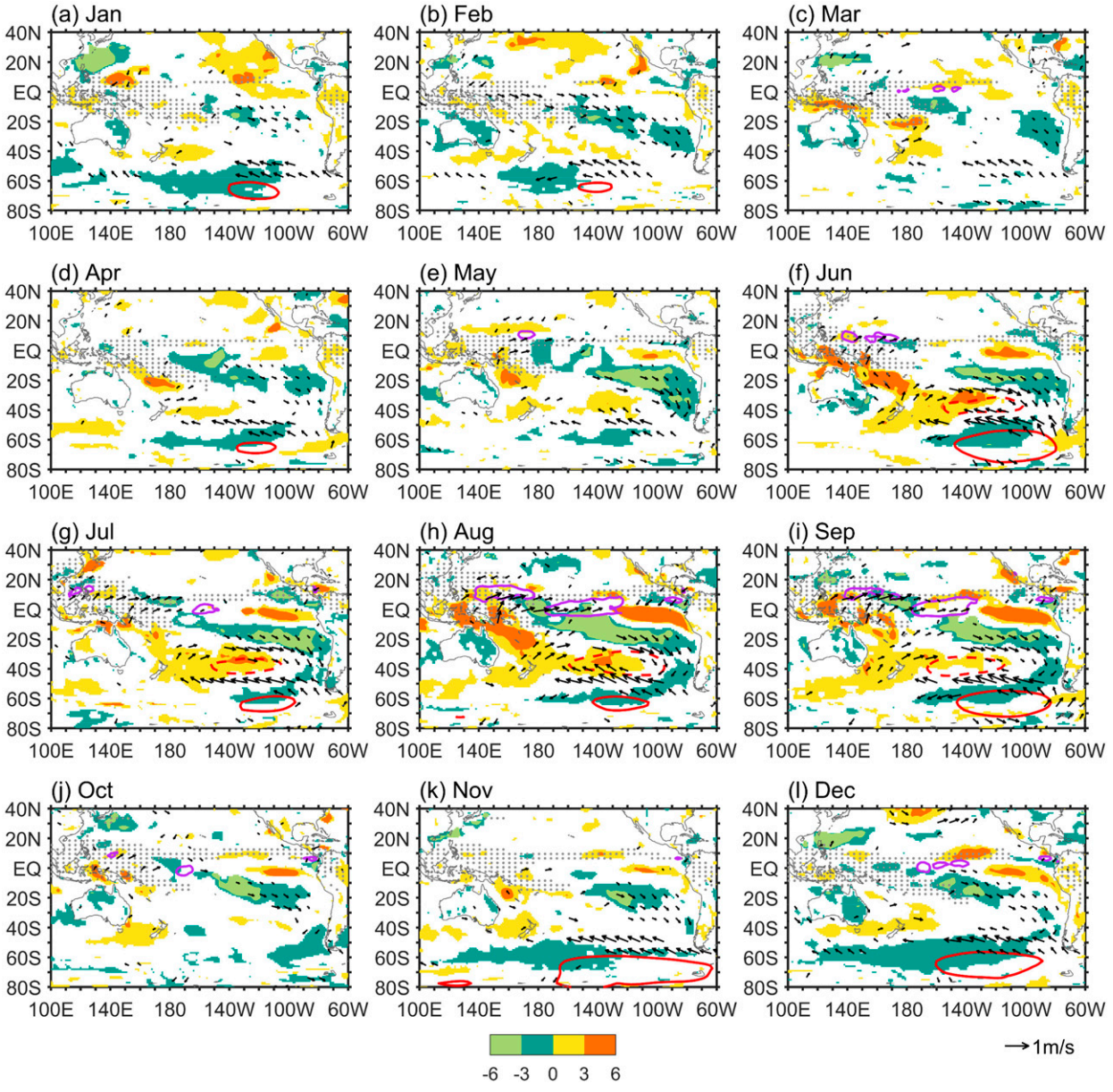

FIG. 6. Regression patterns of interannual latent heat flux anomalies (W m^{-2}; shading; upward positive), SLPAs (hPa; red contours, solid for positive value and dashed for negative value, with an interval of 1), convective precipitation anomalies (mm day^{-1}; violet contours; only 0.4 mm day^{-1} is plotted), and 10-m wind anomalies (m s^{-1}; vectors) onto the simultaneous SPO index. Climatological convective precipitation over 6 mm day^{-1} is indicated by gray dots. Only the correlation coefficients significantly exceeding the 90% confidence level are plotted.

result can explain why the SPO variability is not an effective precursor for the far-eastern Pacific SST variance shown in Capotondi and Ricciardulli (2021).

c. *Relative contributions of the NPO and the SPO*

As the NPO and the SPO affect the interannual variability of the WCEP zonal wind in different seasons, it is important to assess their relative contributions. Overall, the WCEP wind is correlated more closely with the austral winter SPO than the boreal winter NPO, with a correlation coefficient of 0.6 and 0.3, respectively (Fig. 2f). Consequently, the SPO–ENSO connection is stronger than the NPO–ENSO one (Fig. 2g).

We find that the changes in the NITCZ, being important for the equatorial Pacific zonal wind, can be attributed to the NPO in the Northern Hemisphere and the SPO in the Southern Hemisphere. The NPO-related NITCZ not only amplifies the equatorial westerly wind anomalies, but also promotes the equatorward meridional flow to the northeast of the Australian continent that is related to the ACEF (Figs. 4a–f). The NITCZ leads the ACEF by 3 months, with a correlation

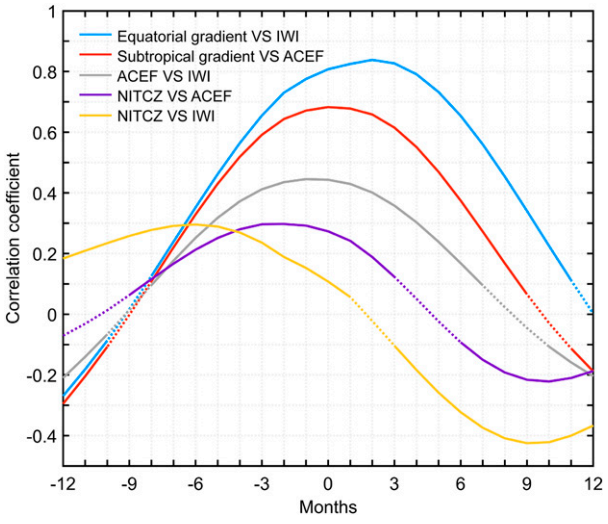

FIG. 7. Lead–lag correlations between JAS-IWI and its possible impacting factors. Legend is presented by "*A* VS *B*." The positive values on the *x* axis indicate *A* lags behind *B*, while the negative values indicate *A* leads *B*. The blue line represents the correlations between IWI and equatorial Pacific SLPAs zonal gradient [difference between the west domain (10°S–10°N, 90°–150°E) and the east domain (10°S–10°N, 180°–90°W)]; gray and yellow lines indicate the correlations between IWI and ACEF (50°–20°S, 160°E–170°W) and NITCZ (5°–20°N, 140°E–180°) anomalies, respectively. The orange and violet lines indicate the correlations between ACEF and South Pacific subtropical SLPAs zonal gradient [difference between the west domain (50°–10°S, 110°–160°E) and the east domain (50°–20°S, 180°–100°W)], NITCZ anomalies, respectively. Significant correlation coefficients at the 90% confidence level based on the two-tailed Student's *t* test are connected by the solid line.

coefficient of 0.3 (Fig. 7, violet line). Meanwhile, the South Pacific subtropical SLP zonal gradient changes simultaneously with the ACEF, with a much higher coefficient of 0.68 (Fig. 7, red line), implying that the ACEF can be modulated by the South Pacific atmospheric variability more efficiently. The subtropical South Pacific SLP zonal gradient can be affected by the SPO. Thus, the SPO can modulate the ACEF once it is energized, especially after the boreal spring (Fig. 2e). Then, these meridional wind anomalies reinforce the NPO-related NITCZ anomalies and continuously influence the WCEP zonal wind in austral winter. Although both the NITCZ and the ACEF lead the JAS-IWI for at least 1 month, the relationship between the ACEF and IWI is stronger. This represents a more significant impact of the South Pacific climate variability on the tropics in austral winter than that from the North Pacific. We further noticed that the changes in the equatorial Pacific zonal SLP gradient lag the JAS-IWI by 3 months (Fig. 7, blue line). This means that the interannual wind is regulated by other factors prior to the equatorial SLP gradient.

The eastward extension of the WCEP zonal wind anomalies is important for the development of ENSO and can be contributed by the SPO, and less so by the NPO. The NPO plays a precursor role in the JAS-IWI, with a lead time of 10–11 months (Fig. 2f), but it could only fluctuate the central equatorial Pacific zonal wind via the PMM and by modulating the NITCZ during boreal winter and spring. Without the SPO, these NPO-related WCEP zonal wind anomalies would be more confined to the west of 150°W (Fig. 4). They even retreat to the west of the international date line in August. It can be noticed that the austral winter SPO is highly related to the interannual wind along the central-eastern equatorial Pacific (Figs. 6h,i), which corresponds to a farther eastward extension of zonal wind anomalies for at least 10°. This study, therefore, illustrates the important role of the SPO in promoting persistent eastern Pacific zonal wind variations, partly explaining why the eastern Pacific ENSO events with large magnitude are more likely to be accompanied by the SPO (You and Furtado 2017; Larson et al. 2018).

As stated above, the extratropical atmospheric forcing from both hemispheres can affect the tropics, but the winter hemisphere signals tend to be more efficient. This may be due to the seasonal phase-locking feature of the interannual atmospheric variations and their interactions with the seasonally varying background winds in both hemispheres. The North Pacific variability possesses a longer lead time ahead of the JAS-IWI, but with a relatively weaker relationship compared with the South Pacific variability. This may come from a variety of reasons, which should be further investigated. Here, we propose three possibilities: (i) In boreal spring, the tropical air–sea interactions are not robust enough to amplify the NPO-related WCEP zonal wind anomalies. (ii) As tropical ocean–atmosphere coupling strengthens during austral winter, the South Pacific extratropical atmospheric signals can be contemporaneously modulated by the tropical air–sea interactions (Hong et al. 2014) and conversely regulate the tropics, constituting a positive feedback loop that reinforces their relationship. Nevertheless, the response of the NPO to the tropical signals will be more visible when boreal winter comes in the next year, and they are negatively correlated with that in the prior year (Fig. 5l). Thus, the interaction between the North Pacific and the tropics is out of phase. (iii) By considering oceanic processes, the strength of tropical–extratropical interactions can benefit from the equatorial Pacific heat content, which has been shown to reach a maximum in the ENSO-developing austral winter (Kug et al. 2009). All these possible reasons account for a more efficient effect of the SPO. Overall, the annual cycle of climatic variability provides two significant extratropical predictors in both hemispheres for the WCEP interannual wind, the NPO and the SPO. They are important precursors for tropical air–sea couplings that should not be neglected in ENSO predictions, although with different efficiencies. Our improved understanding of the WCEP interannual wind motivates research on the predictable capability of these two precursors. An estimated JAS-IWI by using the preceding NPO and SPO indices will be constructed in the next section.

5. Estimated WCEP wind index

The WCEP interannual wind leads ENSO by 3 months, with a correlation coefficient of approximately 0.8, indicating that the austral winter IWI is a key predictor for ENSO. Both the interannual wind and ENSO show seasonal phase-locking

characteristics. The IWI peaks in the late austral winter (Fig. 1d), while ENSO peaks in the boreal winter. However, a lead time of nearly one season is not sufficient for long-lead ENSO predictions. We have shown that the NPO and the SPO are significantly correlated with the JAS-IWI by a lead time of up to 1 year. How predictable is ENSO if we only consider the two extratropical precursors?

To reveal the seasonally alternate roles of the NPO and the SPO in affecting the WCEP interannual wind and ENSO, we propose an empirical predictive model to depict the JAS-IWI using a multiple linear regression method, only based on the NPO index and SPO index (note that the NPO and the SPO are not significantly correlated with each other based on a 12-month lead–lag correlation analysis). It can be expressed by the following equation:

$$\mathrm{IWI}_m^y = \alpha_m \times \mathrm{NPO}^y + \beta_m \times \mathrm{SPO}_m^y + \gamma_m, \qquad (1)$$

where y and m, respectively, represent the given year and month of hindcast; y is from 1948 to 2020, and m is from January to August of every year. The linear regression coefficient of JAS-IWI onto the standardized boreal winter NPO and SPO index in the specific month of m every year can be expressed as α and β_m, respectively; γ_m is the constant term. A JAS-IWI based on the preceding NPO and SPO indices commencing from January to August has thus been constructed, over the period 1948–2020. The regressed coefficients of the SPO change by month, indicating seasonally varying contributions of the extratropical predictor to the tropics. Concentrating on the interannual time scale, the SPO index used in this model has been filtered with a bandpass of 1–9 years as it contains both interannual and multidecadal variations. The NPO indices obtained in two different ways, the $\mathrm{NPO}_{\mathrm{NS}}$ and the $\mathrm{NPO}_{\mathrm{EOF}}$, have been applied in this model. The NPO has a dominant frequency on the interannual time scale, so the results using the filtered and the unfiltered NPO indices are not much different. To test for the robustness and applicability of this predictive model, we randomly split the time series into training groups (40 years) and testing groups (23 years) 1000 times using the Monte Carlo method. Then we compare the $\mathrm{IWI}_{\mathrm{MLR}}$ with the observed one.

The $\mathrm{IWI}_{\mathrm{MLR}}$ shows correspondence with the observed one that we derive using the EEMD method (Figs. 8a,b). It corresponds closely to the observed JAS-IWI, with a long lead time of 6 months. Their correlation coefficient exceeds 0.5 when we use the preceding boreal winter NPO and SPO indices (orange line in January), and displays an ascending tendency as the given time approaches austral winter (Fig. 8). It reaches up to nearly 0.8 in August. The JAS-IWI using the NPO and the SPO as predictors can represent the observed WCEP interannual wind fluctuations reasonably well. However, the correlation between the $\mathrm{IWI}_{\mathrm{MLR}}$ and ENSO is even more significant than that between the $\mathrm{IWI}_{\mathrm{MLR}}$ and the observed JAS-IWI (Figs. 8c,d). This feature implies that the NPO and the SPO affect the central-eastern Pacific SST through other processes, such as oceanic advection. The correlation coefficient between $\mathrm{IWI}_{\mathrm{MLR}}$ and the ENSO index is approximately 0.6 when the wind index is estimated by using the wintertime $\mathrm{NPO}_{\mathrm{NS}}$ and SPO indices (Fig. 8d). This feature means that the NPO and the SPO can be relatively reliable long-lead precursors for ENSO, with a lead time of 1 year. Moreover, the $\mathrm{IWI}_{\mathrm{MLR}}$ based on extratropical climate signals lessens the effect of the spring predictability barrier, as increasing tendencies of the correlation coefficients can be seen in Fig. 8. That might be because tropical air–sea interactions are more susceptible to extratropical signals from boreal spring to early summer than in other seasons.

Significant reductions in the correlation coefficients before April can be noticed when the NPO term is omitted in the $\mathrm{IWI}_{\mathrm{MLR}}$ (Fig. 8c), indicating an indispensable role of the NPO in regulating tropical variability (Figs. 8d,e). As all three estimated JAS-IWI displayed in Fig. 8 contain the variation of the SPO, they tend to be unanimous by approaching August. That is to say, from late boreal spring to austral winter, the influences from the North Pacific rapidly decay, and South Pacific atmospheric signals gradually take over the role of the North Pacific signals in affecting tropical air–sea interactions. The result provides us with input to better predictions of ENSO by further considering extratropical climate variability with seasonally alternate roles.

6. Conclusions and discussion

a. *Conclusions*

The tropical Pacific embeds strong air–sea interactions that energize ENSO events and provides an overlapped region for extratropical climate variability in both hemispheres to exert joint effects on the tropics. The interannual components of the WCEP zonal wind significantly contribute to central-eastern Pacific SST fluctuations, which can be significantly fueled by the NPO in boreal winter–spring and the SPO in austral winter. These two entities of winter hemisphere extratropical variations alternately influence the equatorial Pacific zonal wind by modulating basinwide surface heat flux adjustments and the consequent tropical convective perturbations. The NPO variability, peaking in boreal winter, generates the NPMM in the following seasons, which has been described by the SFM (Chiang and Vimont 2004). On the other hand, the equatorward cyclonic lobe of the NPO promotes tropical convection to the north of the NITCZ and facilitates the northward cross-equatorial winds to the south through a Gill response. These two dynamic–thermodynamic processes are responsible for the NPO-induced variation of WCEP interannual wind. As austral winter approaches, the South Pacific extratropical signals gradually take the role of the North Pacific ones in regulating the tropics. A positive SPO enhances the ACEF and accelerates the heat loss from the sea surface where it prevails to the southwest of the SPCZ. By contrast, it is favorable for heat gain in the southeast tropical Pacific through the SPMM (Fig. 9). These basin-scale air–sea couplings will lead to an equatorward shift of the SPCZ and the central Pacific ITCZ, and then promote eastern equatorial Pacific convection. A strengthened ACEF can also reinforce the NPO-induced changes in the NITCZ and the

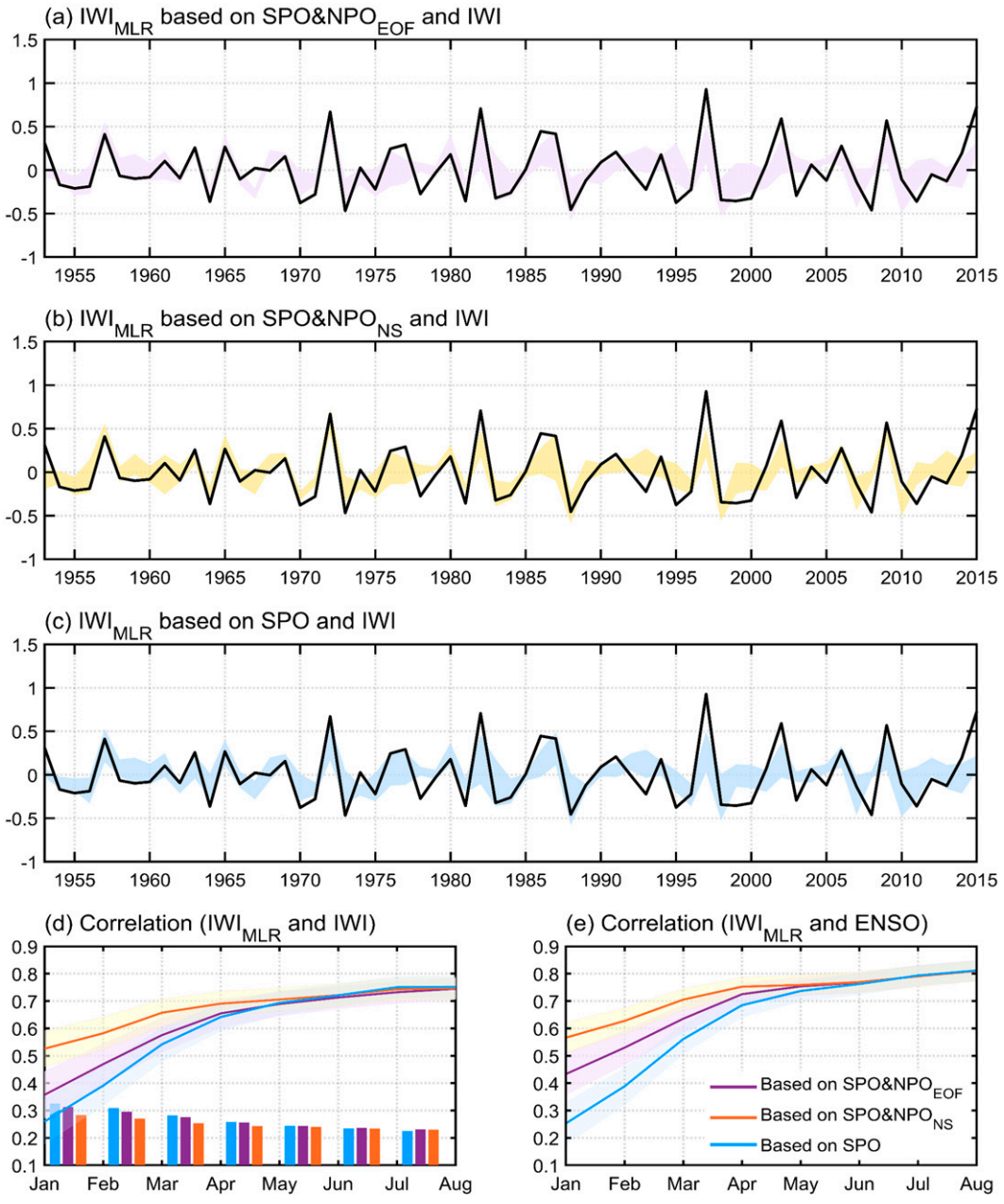

FIG. 8. Observed JAS-IWI and estimated JAS-IWI (IWI_{MLR}) based on the NPO and SPO indices. (a) The IWI_{MLR} based on boreal winter interannual NPO_{EOF} and simultaneous interannual SPO index commencing from January to August is shown by color shading (spanning from the minimum IWI_{MLR} value to the maximum value in each year), while the observed JAS-IWI is shown by the solid black line. (b) As in (a), but the IWI_{MLR} is based on boreal winter interannual NPO_{NS} and simultaneous interannual SPO index. (c) As in (a), except the IWI_{MLR} is only based on simultaneous interannual SPO index. (d) Correlations between IWI and IWI_{MLR} commencing from the specific given month. Solid lines indicate the averaged values of the correlation coefficients in the 1000-time Monte Carlo sampling, and the color shading covers 0.5 standard deviations of the correlation coefficients. Bars indicate the averaged values of all the test root-mean-square errors of the IWI_{MLR}. (e) Correlations between IWI_{MLR} and subsequent boreal winter Niño-3.4 index. We also use the leave-one-out cross-validation method to test the model and get a similar result (not shown).

consequent WCEP zonal wind anomalies. Above all, the NPO and the SPO are key factors for both the WCEP zonal wind and ENSO, following the seasonal cycle of the climate system.

Our wind prediction model, by using the two extratropical climate signals, can well estimate the WCEP interannual wind variations and ENSO. The result shows that the NPO benefits a long-lead prediction of ENSO, while the SPO is the most

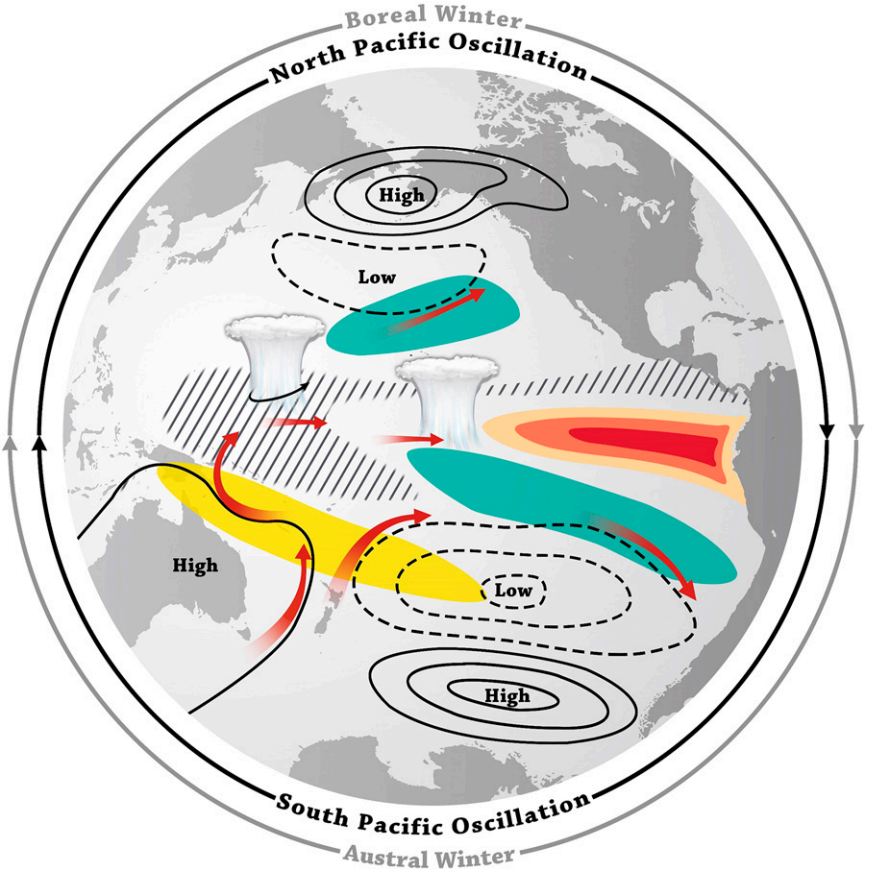

FIG. 9. Schematic diagram showing seasonally alternate winter hemisphere extratropical boosters for the WCEP interannual wind. The black contours indicate the SLPAs in a positive phase of the NPO (in the Northern Hemisphere) and the SPO (in the Southern Hemisphere). Red arrows indicate the anomalous atmospheric surface flows related to the NPO and the SPO. Shading indicates sea surface latent heat exchanges (positive latent heat flux into the underlying sea surface is green and upward to the atmosphere is light yellow). Red shading represents sea surface warming in the ENSO region. Gray hatching represents the climatological rainfall band. The convective rainfall symbol represents the anomalous tropical convection attributed to the NPO and the SPO.

important predictor of ENSO amplitude. Extratropical predictors can help to reduce the spring predictability barrier of ENSO predictions resulting from insufficient precursors within the tropics (also shown in Chen et al. 2020), especially the NPO variability. The SPO is more efficient in affecting the tropics than the NPO, which might be due to the seasonal phase-locking features of the interannual atmospheric variations that have been illustrated in the mechanisms section. Overall, neither of these two extratropical predictors should be omitted in long-lead predictions of ENSO.

b. *Discussion*

ENSO is a basin-scale phenomenon resulting from multiple interactions of climate variations on different time scales. Extratropical atmospheric signals were regarded as high-frequency stochastic forcing for the tropical atmospheric variability and ENSO (e.g., Moore and Kleeman 1999). However, we have shown that the WCEP interannual zonal wind on a lower frequency contributes the most to the variation of tropical Pacific SST, indicating a strong resonance of climate signals on the interannual time scales. The result is in agreement with that of other studies (e.g., Capotondi et al. 2018). The correlation between higher-frequency components and central-eastern equatorial SSTAs is weaker, but this does not mean that the ocean–atmosphere signals, with a time scale shorter than interannual ones, bear no relation to ENSO. It was proposed that the seasonal transition of the Asian–Australian monsoon system could substantially affect the WCEP seasonal zonal wind and the onset time of El Niño (Xu and Chan 2001; Sullivan et al. 2021). Furthermore, Australian cold surges intruding into the western Pacific tropics occur more frequently when the Australian winter monsoon is strong (Stephens et al. 2007). The SPO, which is shown to modulate the Australian winter monsoon (e.g., ACEF) and intimately link to tropical air–sea interactions on interannual time scales in this study, possesses a periodicity of

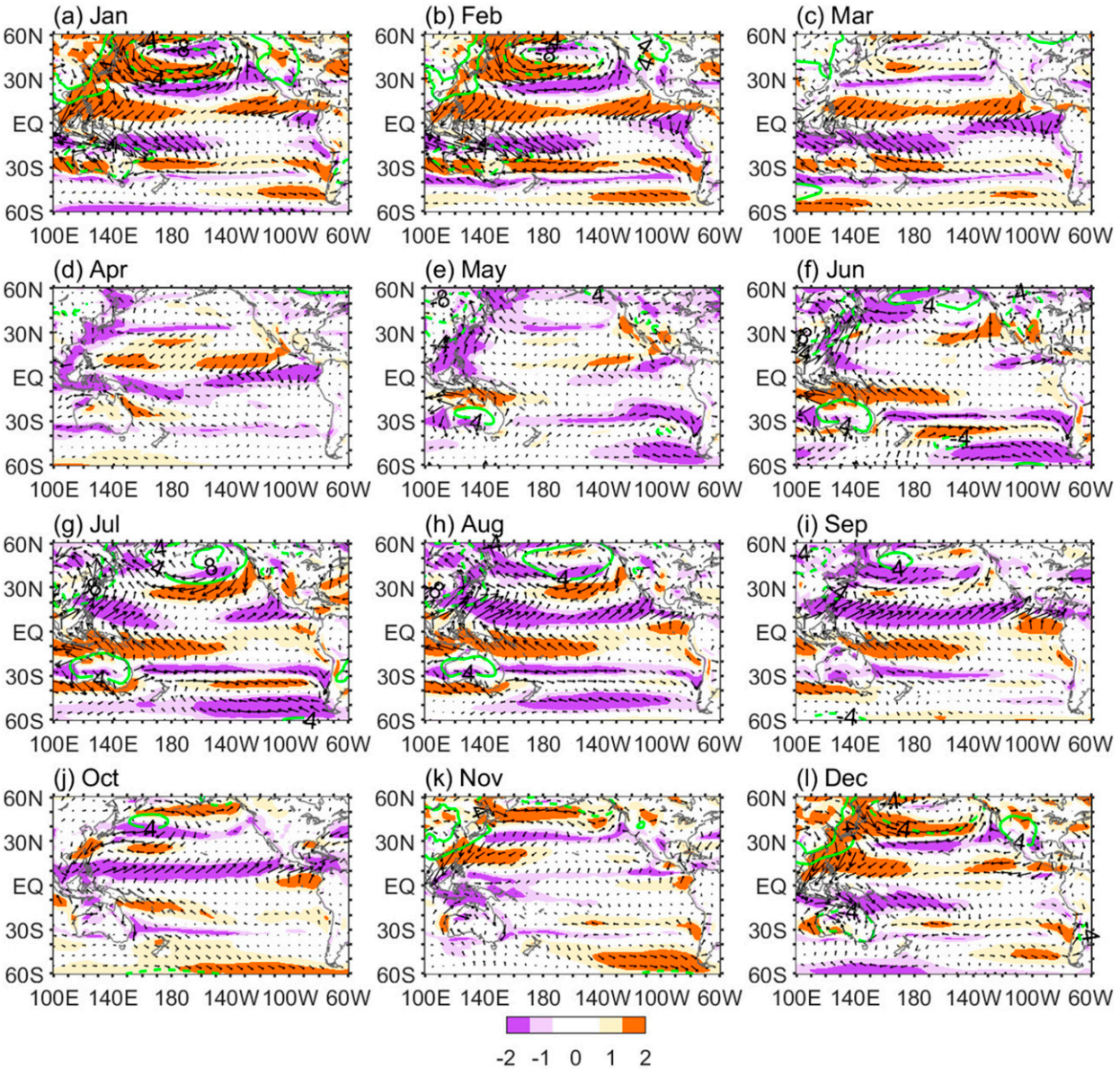

FIG. A1. Climatological annual cycle of the SLP (hPa; green contours), 10-m wind (m s^{-1}; vectors), and 10-m wind speed (m s^{-1}; shading). The climatological annual cycle is calculated by subtracting the annual mean from the climatological value of every month.

4–5 years (not shown). Previous studies have argued that the equatorial Pacific zonal wind modulated by the Asian–Australian monsoon could be strongly coupled with the central-eastern Pacific SST on a nearly 4-yr scale as well (Zhun and Chen 2002). This time scale is consistent with the basin-scale ocean–atmosphere dynamics (Philander 1990; Webster and Yang 1992). Thus, we speculate that the interannual climate variability might provide a low-frequency background that modulates the inclination of high-frequency events, which could conversely feed back to low-frequency climate signals. Thus, our result helps to understand the mechanism for monsoon–ENSO interactions on the interannual time scale.

The mechanisms of the tropical–extratropical interactions responsible for ENSO variability are complex, subject to both atmospheric and oceanic processes. Our work emphasizes how the North Pacific and South Pacific atmospheric signals alternately affect the WCEP interannual wind and ENSO. We notice that the estimated JAS-IWI is better correlated with the observed ENSO SST index than with the wind index (Figs. 8c,d), which may be because the tropical–extratropical ocean heat transport related to the NPO and the SPO provides a favorable condition for the large growth rate of SST anomalies. Several previous studies depicted that the North Pacific climate anomalies can affect the equatorial ocean through oceanic topical–subtropical pathways, especially in the central Pacific (Zhang et al. 1998; Di Lorenzo et al. 2015; Zhu et al. 2021). Moreover, the SPO was perceived as an indicator of the eastern Pacific SST variance, as the SPO-related subtropical atmospheric cyclonic circulation weakens the southeasterly trade winds and charges

the eastern equatorial Pacific (You and Furtado 2018; Liguori and Di Lorenzo 2019). Therefore, the associated changes in upper-ocean flow and heat content not only are responsive to atmospheric forcing, but also provide possible ways to modulate the seasonally alternating interactions that we describe in this study.

Those extratropical–tropical oceanic processes can partly explain ENSO diversity (You and Furtado 2018), somehow different from the impacts of atmospheric variability shown in Capotondi and Ricciardulli (2021). That is, extratropical climate variability can regulate tropical Pacific wind variation and the oceanic condition through both atmospheric and oceanic pathways. Then, the consequent atmospheric changes and oceanic changes conspire to regulate the dynamic processes accounting for different types of ENSO, which has been shown by Fan et al. (2021). Although the austral winter SPO induces a more eastward extension of the interannual wind anomalies, these winds are still confined far away from the South American coast (Fig. 6), implying that the far-eastern Pacific air–sea interactions might be dominated by other factors (e.g., Zhong et al. 2019). This can help to explain why the wind speed modes shown by Capotondi and Ricciardulli (2021) display little correlation to the eastern Pacific ENSO. Our study reveals how the NPO and the SPO take turns to influence the tropics, in concert with atmospheric responses. Tropical convection seems to be the atmospheric hinge of extratropical signals in the two hemispheres, whereas the oceanic one remains to be clarified. A comprehensive description unified with the perspective of oceanic pathways related to extratropical climate signals should be investigated in future studies, especially for predictions of ENSO diversity.

Acknowledgments. This study was supported by the National Key R&D Program of China (2020YFA0608803), the National Natural Science Foundation of China (Grant 42105052), the Guangdong Major Project of Basic and Applied Basic Research (Grant 2020B0301030004), the Guangdong Province Key Laboratory for Climate Change and Natural Disaster Studies (Grant 2020B1212060025), and the Innovation Group Project of Southern Marine Science and Engineering Guangdong Laboratory (Zhuhai) (Grant 311021001).

Data availability statement. NCEP reanalysis data can be obtained from https://www.esrl.noaa.gov/psd/data/gridded/data.ncep.reanalysis.html and https://www.esrl.noaa.gov/psd/data/gridded/data.godas.html. HadISST data are available at https://www.metoffice.gov.uk/hadobs/hadisst. Daily OISST data are from https://www.ncdc.noaa.gov/oisst/data-access. CMAP precipitation data are derived from https://psl.noaa.gov/data/gridded/data.cmap.html. GPCP precipitation data are provided by NOAA/OAR/ESRL PSL, Boulder, Colorado, from their website at https://psl.noaa.gov/data/gridded/data.gpcp.html.

APPENDIX

Climatological Annual Cycle of the Pacific Low-Level Atmospheric Circulation

Figure A1 shows the climatological annual cycle of the SLP and 10-m winds.

REFERENCES

Adler, R. F., and Coauthors, 2003: The Version-2 Global Precipitation Climatology Project (GPCP) monthly precipitation analysis (1979–present). *J. Hydrometeor.*, **4**, 1147–1167, https://doi.org/10.1175/1525-7541(2003)004<1147:TVGPCP>2.0.CO;2.

Amaya, D. J., Y. Kosaka, W. Zhou, Y. Zhang, S.-P. Xie, and A. J. Miller, 2019: The North Pacific pacemaker effect on historical ENSO and its mechanisms. *J. Climate*, **32**, 7643–7661, https://doi.org/10.1175/JCLI-D-19-0040.1.

Anderson, B. T., 2007: On the joint role of subtropical atmospheric variability and equatorial subsurface heat content anomalies in initiating the onset of ENSO events. *J. Climate*, **20**, 1593–1599, https://doi.org/10.1175/JCLI4075.1.

Bartlett, M. S., 1935: Some aspects of the time-correlation problem in regard to tests of significance. *J. Roy. Stat. Soc.*, **98**, 536–543, https://doi.org/10.2307/2342284.

Bergman, J. W., H. H. Hendon, and K. M. Weickmann, 2001: Intraseasonal air–sea interactions at the onset of El Niño. *J. Climate*, **14**, 1702–1719, https://doi.org/10.1175/1520-0442(2001)014<1702:IASIAT>2.0.CO;2.

Bjerknes, J., 1969: Atmospheric teleconnections from the equatorial Pacific. *Mon. Wea. Rev.*, **97**, 163–172, https://doi.org/10.1175/1520-0493(1969)097<0163:ATFTEP>2.3.CO;2.

Cai, W., and Coauthors, 2012: More extreme swings of the South Pacific convergence zone due to greenhouse warming. *Nature*, **488**, 365–369, https://doi.org/10.1038/nature11358.

——, and Coauthors, 2015: ENSO and greenhouse warming. *Nat. Climate Change*, **5**, 849–859, https://doi.org/10.1038/nclimate2743.

——, B. Ng, T. Geng, L. Wu, A. Santoso, and M. J. McPhaden, 2020: Butterfly effect and a self-modulating El Niño response to global warming. *Nature*, **585**, 68–73, https://doi.org/10.1038/s41586-020-2641-x.

Capotondi, A., and L. Ricciardulli, 2021: The influence of Pacific winds on ENSO diversity. *Sci. Rep.*, **11**, 18672, https://doi.org/10.1038/s41598-021-97963-4.

——, P. D. Sardeshmukh, and L. Ricciardulli, 2018: The nature of the stochastic wind forcing of ENSO. *J. Climate*, **31**, 8081–8099, https://doi.org/10.1175/JCLI-D-17-0842.1.

Chang, P., L. Zhang, R. Saravanan, D. J. Vimont, J. C. H. Chiang, L. Ji, H. Seidel, and M. K. Tippett, 2007: Pacific meridional mode and El Niño–Southern Oscillation. *Geophys. Res. Lett.*, **34**, L16608, https://doi.org/10.1029/2007GL030302.

Chen, D., and Coauthors, 2015: Strong influence of westerly wind bursts on El Niño diversity. *Nat. Geosci.*, **8**, 339–345, https://doi.org/10.1038/ngeo2399.

Chen, H.-C., Y.-H. Tseng, Z.-Z. Hu, and R. Ding, 2020: Enhancing the ENSO predictability beyond the spring barrier. *Sci. Rep.*, **10**, 984, https://doi.org/10.1038/s41598-020-57853-7.

Chen, S., and R. Wu, 2018: Impacts of winter NPO on subsequent winter ENSO: Sensitivity to the definition of NPO index. *Climate Dyn.*, **50**, 375–389, https://doi.org/10.1007/s00382-017-3615-z.

Chiang, J. C. H., and D. J. Vimont, 2004: Analogous Pacific and Atlantic meridional modes of tropical atmosphere–ocean variability. *J. Climate*, **17**, 4143–4158, https://doi.org/10.1175/JCLI4953.1.

Chiodi, A. M., D. E. Harrison, and G. A. Vecchi, 2014: Subseasonal atmospheric variability and El Niño waveguide warming: Observed effects of the Madden–Julian oscillation and westerly wind events. *J. Climate*, **27**, 3619–3642, https://doi.org/10.1175/JCLI-D-13-00547.1.

Christensen, H. M., J. Berner, D. R. B. Coleman, and T. N. Palmer, 2017: Stochastic parameterization and El Niño–Southern

Oscillation. *J. Climate*, **30**, 17–38, https://doi.org/10.1175/JCLI-D-16-0122.1.

Chu, P.-S., 1988: Extratropical forcing and the burst of equatorial westerlies in the western Pacific: A synoptic study. *J. Meteor. Soc. Japan*, **66**, 549–564, https://doi.org/10.2151/jmsj1965.66.4_549.

Chu, T.-Y., and W.-C. Huang, 2020: Application of empirical mode decomposition method to synthesize flow data: A case study of Hushan reservoir in Taiwan. *Water*, **12**, 927, https://doi.org/10.3390/w12040927.

Di Lorenzo, E., G. Liguori, N. Schneider, J. C. Furtado, B. T. Anderson, and M. A. Alexander, 2015: ENSO and meridional modes: A null hypothesis for Pacific climate variability. *Geophys. Res. Lett.*, **42**, 9440–9448, https://doi.org/10.1002/2015GL066281.

Ding, R., J. Li, and Y.-H. Tseng, 2015: The impact of South Pacific extratropical forcing on ENSO and comparisons with the North Pacific. *Climate Dyn.*, **44**, 2017–2034, https://doi.org/10.1007/s00382-014-2303-5.

——, ——, ——, C. Sun, and F. Xie, 2017: Joint impact of North and South Pacific extratropical atmospheric variability on the onset of ENSO events. *J. Geophys. Res. Atmos.*, **122**, 279–298, https://doi.org/10.1002/2016JD025502.

Eisenman, I., L. Yu, and E. Tziperman, 2005: Westerly wind bursts: ENSO's tail rather than the dog? *J. Climate*, **18**, 5224–5238, https://doi.org/10.1175/JCLI3588.1.

Fan, H., B. Huang, S. Yang, and W. Dong, 2021: Influence of the Pacific meridional mode on ENSO evolution and predictability: Asymmetric modulation and ocean preconditioning. *J. Climate*, **34**, 1881–1901, https://doi.org/10.1175/JCLI-D-20-0109.1.

Fasullo, J., and P. J. Webster, 2000: Atmospheric and surface variations during westerly wind bursts in the tropical western Pacific. *Quart. J. Roy. Meteor. Soc.*, **126**, 899–924, https://doi.org/10.1002/qj.49712656407.

Flandrin, P., G. Rilling, and P. Goncalves, 2004: Empirical mode decomposition as a filter bank. *IEEE Signal Process. Lett.*, **11**, 112–114, https://doi.org/10.1109/LSP.2003.821662.

Fu, M., and E. Tziperman, 2019: Essential ingredients to the dynamics of westerly wind bursts. *J. Climate*, **32**, 5549–5565, https://doi.org/10.1175/JCLI-D-18-0584.1.

Furtado, J. C., E. Di Lorenzo, B. T. Anderson, and N. Schneider, 2012: Linkages between the North Pacific Oscillation and central tropical Pacific SSTs at low frequencies. *Climate Dyn.*, **39**, 2833–2846, https://doi.org/10.1007/s00382-011-1245-4.

Gebbie, G., and E. Tziperman, 2008: Predictability of SST-modulated westerly wind bursts. *J. Climate*, **22**, 3894–3909, https://doi.org/10.1175/2009JCLI2516.1.

Gill, A. E., 1980: Some simple solutions for heat-induced tropical circulation. *Quart. J. Roy. Meteor. Soc.*, **106**, 447–462, https://doi.org/10.1002/qj.49710644905.

Harrison, D. E., and G. A. Vecchi, 1997: Westerly wind events in the tropical Pacific, 1986–95. *J. Climate*, **10**, 3131–3156, https://doi.org/10.1175/1520-0442(1997)010<3131:WWEITT>2.0.CO;2.

Hendon, H. H., M. C. Wheeler, and C. Zhang, 2007: Seasonal dependence of the MJO–ENSO relationship. *J. Climate*, **20**, 531–543, https://doi.org/10.1175/JCLI4003.1.

Hong, L.-C., L. Ho, and F.-F. Jin, 2014: A Southern Hemisphere booster of super El Niño. *Geophys. Res. Lett.*, **41**, 2142–2149, https://doi.org/10.1002/2014GL059370.

Huang, N. E., and Coauthors, 1998: The empirical mode decomposition and Hilbert spectrum for nonlinear and non-stationary time series analysis. *Proc. Roy. Soc. London*, **454A**, 903–995, https://doi.org/10.1098/rspa.1998.0193.

——, Z. Shen, and S. R. Long, 1999: A new view of nonlinear water waves: The Hilbert spectrum. *Annu. Rev. Fluid Mech.*, **31**, 417–457, https://doi.org/10.1146/annurev.fluid.31.1.417.

Kalnay, E., and Coauthors, 1996: The NCEP/NCAR 40-Year Reanalysis Project. *Bull. Amer. Meteor. Soc.*, **77**, 437–471, https://doi.org/10.1175/1520-0477(1996)077<0437:TNYRP>2.0.CO;2.

Karoly, D. J., 1989: Southern Hemisphere circulation features associated with El Niño–Southern Oscillation events. *J. Climate*, **2**, 1239–1252, https://doi.org/10.1175/1520-0442(1989)002<1239:SHCFAW>2.0.CO;2.

Keen, R. A., 1982: The role of cross-equatorial tropical cyclone pairs in the Southern Oscillation. *Mon. Wea. Rev.*, **110**, 1405–1416, https://doi.org/10.1175/1520-0493(1982)110<1405:TROCET>2.0.CO;2.

Kessler, W. S., and R. Kleeman, 2000: Rectification of the Madden–Julian oscillation into the ENSO cycle. *J. Climate*, **13**, 3560–3575, https://doi.org/10.1175/1520-0442(2000)013<3560:ROTMJO>2.0.CO;2.

——, M. J. McPhaden, and K. M. Weickmann, 1995: Forcing of intraseasonal Kelvin waves in the equatorial Pacific. *J. Geophys. Res.*, **100**, 10 613–10 631, https://doi.org/10.1029/95JC00382.

Kug, J.-S., F.-F. Jin, and S.-I. An, 2009: Two types of El Niño events: Cold tongue El Niño and warm pool El Niño. *J. Climate*, **22**, 1499–1515, https://doi.org/10.1175/2008JCLI2624.1.

Larson, S. M., K. V. Pegion, and B. P. Kirtman, 2018: The South Pacific meridional mode as a thermally driven source of ENSO amplitude modulation and uncertainty. *J. Climate*, **31**, 5127–5145, https://doi.org/10.1175/JCLI-D-17-0722.1.

Lau, K.-M., and S. Yang, 1996: The Asian monsoon and predictability of the tropical ocean–atmosphere system. *Quart. J. Roy. Meteor. Soc.*, **122**, 945–957, https://doi.org/10.1002/qj.49712253208.

Li, C., 1990: Interaction between anomalous winter monsoon in East Asia and El Niño events. *Adv. Atmos. Sci.*, **7**, 36–46, https://doi.org/10.1007/BF02919166.

——, and S. Li, 2014: Interannual seesaw between the Somali and the Australian cross-equatorial flows and its connection to the East Asian summer monsoon. *J. Climate*, **27**, 3966–3981, https://doi.org/10.1175/JCLI-D-13-00288.1.

Li, Z., and S. Yang, 2017: Influences of spring-to-summer sea surface temperatures over different Indian Ocean domains on the Asian summer monsoon. *Asia-Pac. J. Atmos. Sci.*, **53**, 471–487, https://doi.org/10.1007/s13143-017-0050-3.

——, ——, C.-Y. Tam, and C. Hu, 2021: Strengthening western equatorial Pacific and Maritime Continent atmospheric convection and its modulation on the trade wind during spring of 1901–2010. *Int. J. Climatol.*, **41**, 1455–1464, https://doi.org/10.1002/joc.6856.

Lian, T., Y. Tang, L. Zhou, S. Ul Islam, C. Zhang, X. Li, and Z. Ling, 2018: Westerly wind bursts simulated in CAM4 and CCSM4. *Climate Dyn.*, **50**, 1353–1371, https://doi.org/10.1007/s00382-017-3689-7.

——, J. Ying, H.-L. Ren, C. Zhang, T. Liu, and X.-X. Tan, 2019: Effects of tropical cyclones on ENSO. *J. Climate*, **32**, 6423–6443, https://doi.org/10.1175/JCLI-D-18-0821.1.

Liguori, G., and E. Di Lorenzo, 2019: Separating the North and South Pacific meridional modes contributions to ENSO and tropical decadal variability. *Geophys. Res. Lett.*, **46**, 906–915, https://doi.org/10.1029/2018GL080320.

Linkin, M. E., and S. Nigam, 2008: The North Pacific Oscillation–west Pacific teleconnection pattern: Mature-phase structure and winter impacts. *J. Climate*, **21**, 1979–1997, https://doi.org/10.1175/2007JCLI2048.1.

Luther, D. S., D. E. Harrison, and R. A. Knox, 1983: Zonal winds in the central equatorial Pacific and El Niño. *Science*, **222**, 327–330, https://doi.org/10.1126/science.222.4621.327.

McPhaden, M. J., F. Bahr, Y. Du Penhoat, E. Firing, S. P. Hayes, P. P. Niiler, P. L. Richardson, and J. M. Toole, 1992: The response of the western equatorial Pacific Ocean to westerly wind bursts during November 1989 to January 1990. *J. Geophys. Res.*, **97**, 14 289–14 303, https://doi.org/10.1029/92JC01197.

Min, Q., and R. Zhang, 2020: The contribution of boreal spring South Pacific atmospheric variability to El Niño occurrence. *J. Climate*, **33**, 8301–8313, https://doi.org/10.1175/JCLI-D-20-0122.1.

——, J. Su, and R. Zhang, 2017: Impact of the South and North Pacific meridional modes on the El Niño–Southern Oscillation: Observational analysis and comparison. *J. Climate*, **30**, 1705–1720, https://doi.org/10.1175/JCLI-D-16-0063.1.

Mo, K. C., 2000: Relationships between low-frequency variability in the Southern Hemisphere and sea surface temperature anomalies. *J. Climate*, **13**, 3599–3610, https://doi.org/10.1175/1520-0442(2000)013<3599:RBLFVI>2.0.CO;2.

Moore, A. M., and R. Kleeman, 1999: Stochastic forcing of ENSO by the intraseasonal oscillation. *J. Climate*, **12**, 1199–1220, https://doi.org/10.1175/1520-0442(1999)012<1199:SFOEBT>2.0.CO;2.

Paek, H., J.-Y. Yu, F. Zheng, and M.-M. Lu, 2019: Impacts of ENSO diversity on the western Pacific and North Pacific subtropical highs during boreal summer. *Climate Dyn.*, **52**, 7153–7172, https://doi.org/10.1007/s00382-016-3288-z.

Park, J.-Y., S.-W. Yeh, J.-S. Kug, and J. Yoon, 2013: Favorable connections between seasonal footprinting mechanism and El Niño. *Climate Dyn.*, **40**, 1169–1181, https://doi.org/10.1007/s00382-012-1477-y.

Pegion, K., C. M. Selman, S. Larson, J. C. Furtado, and E. J. Becker, 2020: The impact of the extratropics on ENSO diversity and predictability. *Climate Dyn.*, **54**, 4469–4484, https://doi.org/10.1007/s00382-020-05232-3.

Philander, S. G., 1990: *El Niño, La Niña, and the Southern Oscillation*. International Geophysics Series, Vol. 46, Academic Press, 293 pp.

Rayner, N. A., D. E. Parker, E. B. Horton, C. K. Folland, L. V. Alexander, D. P. Rowell, E. C. Kent, and A. Kaplan, 2003: Global analyses of sea surface temperature, sea ice, and night marine air temperature since the late nineteenth century. *J. Geophys. Res.*, **108**, 4407, https://doi.org/10.1029/2002JD002670.

Reynolds, R. W., 1993: Impact of Mount Pinatubo aerosols on satellite-derived sea surface temperatures. *J. Climate*, **6**, 768–774, https://doi.org/10.1175/1520-0442(1993)006<0768:IOMPAO>2.0.CO;2.

Rilling, G., and P. Flandrin, 2008: One or two frequencies? The empirical mode decomposition answers. *IEEE Trans. Signal Process.*, **56**, 85–95, https://doi.org/10.1109/TSP.2007.906771.

Rogers, J. C., 1981: The North Pacific Oscillation. *Int. J. Climatol.*, **1**, 39–57, https://doi.org/10.1002/joc.3370010106.

Roulston, M. S., and J. D. Neelin, 2000: The response of an ENSO model to climate noise, weather noise, and intraseasonal forcing. *Geophys. Res. Lett.*, **27**, 3723–3726, https://doi.org/10.1029/2000GL011941.

Seiki, A., and Y. N. Takayabu, 2007: Westerly wind bursts and their relationship with intraseasonal variations and ENSO. Part I: Statistics. *Mon. Wea. Rev.*, **135**, 3325–3345, https://doi.org/10.1175/MWR3477.1.

——, ——, T. Yasuda, N. Sato, C. Takahashi, K. Yoneyama, and R. Shirooka, 2011: Westerly wind bursts and their relationship with ENSO in CMIP3 models. *J. Geophys. Res.*, **116**, D03303, https://doi.org/10.1029/2010JD015039.

Stephens, D. J., M. J. Meuleners, H. van Loon, M. H. Lamond, and N. P. Telcik, 2007: Differences in atmospheric circulation between the development of weak and strong warm events in the Southern Oscillation. *J. Climate*, **20**, 2191–2209, https://doi.org/10.1175/JCLI4131.1.

Stuecker, M. F., 2018: Revisiting the Pacific meridional mode. *Sci. Rep.*, **8**, 3216, https://doi.org/10.1038/s41598-018-21537-0.

Sullivan, A., and Coauthors, 2021: Generation of westerly wind bursts by forcing outside the tropics. *Sci. Rep.*, **11**, 912, https://doi.org/10.1038/s41598-020-79655-7.

Tan, X., Y. Tang, T. Lian, Z. Yao, X. Li, and D. Chen, 2020: A study of the effects of westerly wind bursts on ENSO based on CESM. *Climate Dyn.*, **54**, 885–899, https://doi.org/10.1007/s00382-019-05034-2.

Timmermann, A., and Coauthors, 2018: El Niño–Southern Oscillation complexity. *Nature*, **559**, 535–545, https://doi.org/10.1038/s41586-018-0252-6.

Tziperman, E., and L. Yu, 2007: Quantifying the dependence of westerly wind bursts on the large-scale tropical Pacific SST. *J. Climate*, **20**, 2760–2768, https://doi.org/10.1175/JCLI4138a.1.

Vimont, D. J., D. S. Battisti, and A. C. Hirst, 2001: Footprinting: A seasonal connection between the tropics and mid-latitudes. *Geophys. Res. Lett.*, **28**, 3923–3926, https://doi.org/10.1029/2001GL013435.

——, ——, and ——, 2003a: The seasonal footprinting mechanism in the CSIRO general circulation models. *J. Climate*, **16**, 2653–2667, https://doi.org/10.1175/1520-0442(2003)016<2653:TSFMIT>2.0.CO;2.

——, J. M. Wallace, and D. S. Battisti, 2003b: The seasonal footprinting mechanism in the Pacific: Implications for ENSO. *J. Climate*, **16**, 2668–2675, https://doi.org/10.1175/1520-0442(2003)016<2668:TSFMIT>2.0.CO;2.

——, M. Alexander, and A. Fontaine, 2009: Midlatitude excitation of tropical variability in the Pacific: The role of thermodynamic coupling and seasonality. *J. Climate*, **22**, 518–534, https://doi.org/10.1175/2008JCLI2220.1.

Wallace, J. M., and D. S. Gutzler, 1981: Teleconnections in the geopotential height field during the Northern Hemisphere winter. *Mon. Wea. Rev.*, **109**, 784–812, https://doi.org/10.1175/1520-0493(1981)109<0784:TITGHF>2.0.CO;2.

Webster, P. J., and S. Yang, 1992: Monsoon and ENSO: Selectively interactive systems. *Quart. J. Roy. Meteor. Soc.*, **118**, 877–926, https://doi.org/10.1002/qj.49711850705.

Wu, Z., and N. E. Huang, 2004: A study of the characteristics of white noise using the empirical mode decomposition method. *Proc. Roy. Soc. London*, **460A**, 1597–1611, https://doi.org/10.1098/rspa.2003.1221.

——, and ——, 2009: Ensemble empirical mode decomposition: A noise-assisted data analysis method. *Adv. Adapt. Data Anal.*, **1**, 1–41, https://doi.org/10.1142/S1793536909000047.

Xie, P., and P. A. Arkin, 1997: Global precipitation: A 17-year monthly analysis based on gauge observations, satellite estimates, and numerical model outputs. *Bull. Amer. Meteor. Soc.*, **78**, 2539–2558, https://doi.org/10.1175/1520-0477(1997)078<2539:GPAYMA>2.0.CO;2.

Xie, S.-P., and S. G. H. Philander, 1994: A coupled ocean-atmosphere model of relevance to the ITCZ in the eastern Pacific. *Tellus*, **46A**, 340–350, https://doi.org/10.3402/tellusa.v46i4.15484.

Xu, J., and J. C. L. Chan, 2001: The role of the Asian–Australian monsoon system in the onset time of El Niño events. *J. Climate*, **14**, 418–433, https://doi.org/10.1175/1520-0442(2001)014<0418:TROTAA>2.0.CO;2.

Yeh, S.-W., and B. P. Kirtman, 2004: The North Pacific Oscillation–ENSO and internal atmospheric variability. *Geophys. Res. Lett.*, **31**, L13206, https://doi.org/10.1029/2004GL019983.

You, Y., and J. C. Furtado, 2017: The role of South Pacific atmospheric variability in the development of different types of ENSO. *Geophys. Res. Lett.*, **44**, 7438–7446, https://doi.org/10.1002/2017GL073475.

——, and ——, 2018: The South Pacific meridional mode and its role in tropical Pacific climate variability. *J. Climate*, **31**, 10 141–10 163, https://doi.org/10.1175/JCLI-D-17-0860.1.

——, and ——, 2019: The relationship between South Pacific atmospheric internal variability and ENSO in the North American multimodel ensemble phase-II models. *Geophys. Res. Lett.*, **46**, 12 398–12 407, https://doi.org/10.1029/2019GL084637.

Yu, J.-Y., and S. T. Kim, 2011: Relationships between extratropical sea level pressure variations and the central Pacific and eastern Pacific types of ENSO. *J. Climate*, **24**, 708–720, https://doi.org/10.1175/2010JCLI3688.1.

——, H.-Y. Kao, and T. Lee, 2010: Subtropics-related interannual sea surface temperature variability in the central equatorial Pacific. *J. Climate*, **23**, 2869–2884, https://doi.org/10.1175/2010JCLI3171.1.

Yu, L., R. A. Weller, and W. T. Liu, 2003: Case analysis of a role of ENSO in regulating the generation of westerly wind bursts in the western equatorial Pacific. *J. Geophys. Res.*, **108**, 3128, https://doi.org/10.1029/2002JC001498.

Zhang, C., 1996: Atmospheric intraseasonal variability at the surface in the tropical western Pacific Ocean. *J. Atmos. Sci.*, **53**, 739–758, https://doi.org/10.1175/1520-0469(1996)053<0739:AIVATS>2.0.CO;2.

Zhang, H., A. Clement, and P. Di Nezio, 2014: The South Pacific meridional mode: A mechanism for ENSO-like variability. *J. Climate*, **27**, 769–783, https://doi.org/10.1175/JCLI-D-13-00082.1.

Zhang, R.-H., L. M. Rothstein, and A. J. Busalacchi, 1998: Origin of upper-ocean warming and El Niño change on decadal scales in the tropical Pacific Ocean. *Nature*, **391**, 879–883, https://doi.org/10.1038/36081.

Zhong, W., W. Cai, X.-T. Zheng, and S. Yang, 2019: Unusual anomaly pattern of the 2015/2016 extreme El Niño induced by the 2014 warm condition. *Geophys. Res. Lett.*, **46**, 14 772–14 781, https://doi.org/10.1029/2019GL085681.

Zhu, Y., R.-H. Zhang, D. Li, and D. Chen, 2021: The thermocline biases in the tropical North Pacific and their attributions. *J. Climate*, **34**, 1635–1648, https://doi.org/10.1175/JCLI-D-20-0675.1.

Zhun, Y. F., and L. X. Chen, 2002: The relationship between the Asian/Australian monsoon and ENSO on a quasi-four-year scale. *Adv. Atmos. Sci.*, **19**, 727–740, https://doi.org/10.1007/s00376-002-0012-1.